Transpressive strain partitioning between the Major Gercino Shear Zone and the Tijucas Fold Belt, Dom Feliciano Belt, Santa Catarina, southern Brazil

De Toni, GB[1]*; Bitencourt, MF[2]; Konopásek, J[3,4]; Martini, A[5,6]; Andrade, PHS[7]; Florisbal, LM[8]; Campos, RS[9]

[1,5,7]Programa de Pós Graduação em Geociências, Universidade Federal do Rio Grande do Sul, Av. Bento Gonçalves, 9500, Porto Alegre, 91500-000, RS, Brazil. E-mail: [7]pedrohgeo@hotmail.com

[2]Departamento de Geologia, Universidade Federal do Rio Grande do Sul, Av. Bento Gonçalves, 9500, Porto Alegre, 91500-000, RS, Brazil Brazil. E-mail: fatimab@ufrgs.br

[3]Department of Geosciences, UiT – The Arctic University of Norway in Tromsø, Postboks 6050 Langnes 9037, Tromsø, Norway. E-mail: jiri.konopasek@uit.no

[4]Czech Geological Survey, Klárov 3, 118 21, Prague, Czech Republic

[6]Present address: Instituto de Ciência e Tecnologia, Universidade Federal dos Vales do Jequitinhonha e Mucuri, Rodovia MGT 367 – Km 583, n° 5000, 39100-000, Diamantina, MG, Brazil. E-mail: amosmartini@gmail.com

[8,9]Departamento de Geologia, Universidade Federal de Santa Catarina, R. Eng. Agronômico Andrei Cristian Ferreira, 240-432, Florianópolis, SC, Brazil. E-mail: [8]geoluana@yahoo.com.br; [9]beto.decampos@gmail.com

* Corresponding author. E-mail: gdetoni@ufrgs.br; Phones: +5551991177911; +555133086371

Keywords: Transpression; Strain partitioning; Oblique collision; Cross section

Abstract

A composite cross section from the Florianópolis Batholith towards the Tijucas Fold Belt in the northern Dom Feliciano Belt (southern Brazil) is divided in three structural domains: the Major Gercino Shear Zone, the suprastructural Brusque Complex and the infrastructural Camboriú Complex. A kinematic correlation among the structural domains is based on structural and petrological data integrated with geochronology. An oblique collisional event at 650-645 Ma affected all structural domains and is best recorded in the Porto Belo Complex, which shows migmatization (700°C/4.3 kbar) and top-to-the-NNW+dextral shear along the

Major Gercino Shear Zone. Subsequent strain partitioning led to progressive tangential movement recorded in the Quatro Ilhas Granitoids (625-615 Ma) followed by later granitic intrusions (after 615 Ma) controlled by dextral strike-slip. Meanwhile, the contractional component was absorbed by the Tijucas Fold Belt infrastructure, causing exhumation of the Camboriú Complex migmatites (from 5 to 3.4 kbar) and unroofing of the suprastructural Brusque Complex (around 635 Ma). Tectonic juxtaposition occurred along a dextral+normal detatchment zone between the complexes. As a consequence, heating of the Brusque Complex locally reached amphibolite-facies conditions and suprastructure thrusting inverted to extension, which is recorded in discrete shear structures with normal kinematics. The sequence of events and their age suggest that the hinterland Porto Belo Complex and the foreland Tijucas Fold Belt were juxtaposed already at ca. 650–645 Ma, which questions the validity of the subduction-related tectonic models in the northern Dom Feliciano Belt.

1. Introduction

Most of the present-day plate tectonic boundaries are activated obliquely (Philippon and Corti, 2016). Convergent or divergent oblique displacement vectors are the inevitable consequence of irregular plates moving over the approximately spherical surface of the planet. Obliquely moving plate boundaries are common in almost any segment of every collisional orogenic belt, along active subduction margins, and in restraining bends of faults, shear zones and transform boundaries (Dewey et al., 1998).

Obliquity of the convergence vector with respect to a plate boundary or high-strain zone is the main reason for transpressional deformation (Harland, 1971; Sanderson and Marchini, 1984). Transpression is defined as "what happens to a tabular zone submitted to both compression and (simple) shear simultaneously imposed by its walls" (Robin and Cruden, 1994). The understanding of transpressional deformation evolved through the coupled development of more accurate and increasingly complex mathematical models (Fossen and Tikoff, 1993; Tikoff and Teyssier, 1994; Robin and Cruden, 1994; Jones et al., 2004; Fernández and Diaz-Azpiroz, 2009) and the description of natural occurrences (Holdsworth et al., 2002; Czeck and Hudleston, 2003; Egydio-Silva et al., 2005; Zibra et al., 2014; Martil, 2016; Oriolo et al., 2016).

The distinction of wrench-dominated transpression and pure-shear dominated transpression was introduced by Fossen and Tikoff (1993) and Tikoff and Teyssier (1994). These authors also discussed the importance of coupling between both sides of the collision zone in depth, given by the consistency of the obliquity of the structures observed up to 300 km away from California and Sumatra faults (Tikoff and Teyssier, 1994). Strain partitioning can distribute transpressional deformation in relatively homogeneous structural domains which may coexist laterally (e.g. Holdsworth et al., 2002) or vertically (e.g. Vanderhaeghe et al., 1999), and depends on convergence obliquity (Tikoff and Teyssier, 1994; Robin and Cruden, 1994).

Jones et al. (2004) introduced the concept of inclined transpression, considering non-vertical shear zone walls in a mathematical model based on structures exposed in Eyemouth, SE Scotland (described in detail by Holdsworth et al., 2002). Jones et al. (2004) pointed out the non-coaxiality of thrust and transcurrence components and changes in orientation of the instantaneous strain ellipsoid axis. The presence of kinematic indicators in both XZ and YZ sections, the possibility of non-coaxial structures inside the XY plane due to X reorientation, and the change of vorticity sense during the rock deformation history are consequences predicted in their model. Another feature is the presence of a relative normal-sense of shear in the hanging wall due to the vertical extrusion of matter from the inner portion of the shear zone (Jones et al., 2004), somehow similar to the relative movements of the Main Central Thrust and the South Tibet Detachment in the Himalaya (Burchfiel et al., 1992), with resultant extrusion as the one reported for the Orogen Core of the Kaoko Belt (Goscombe et al., 2005). Fernández and Diaz-Azpiroz (2009) presented an improved model called triclinic transpression with inclined extrusion. They predicted many of observed natural features of transpressional shear zones, as distribution of lineations along girdles or their double plunge. The non-coincidence of the vorticity vector with any of the finite strain axis is characteristic of oblique, triclinic transpression (Fernández and Diaz-Azpiroz, 2009).

This paper presents a structural research integrated with petrological and previously published geochronological data from the northernmost segment of the Dom Feliciano Belt (DFB – Fig. 1), Santa Catarina state (SC), southern Brazil. This is the mobile belt adjacent to the Rio de la Plata Craton and represents the South American portion of the Dom Feliciano-Kaoko-Gariep Orogenic System active during the western Gondwana assembly (Konopásek et al., 2016, 2018 – Fig. 1a). The study investigates and proposes a kinematic correlation between the two major tectonic domains of DFB (Fig. 1b) in SC (figures 1c and 2), separated hereby in three structural domains: (i) the northernmost portion of the Florianópolis Batholith (defined by Jost and Hartmann, 1984), which was affected by the Major Gercino Shear Zone (MGSZ –Bitencourt and Nardi, 1993, 2000; Bitencourt, 1996; Florisbal et al., 2012a; Hueck et al., 2018) that separates the batholith from the Tijucas Fold Belt (TFB – as defined by Hasui et al., 1975). The TFB in the northern Dom Feliciano Belt is represented by (ii) the supracrustal Brusque Complex (Silva, 1991; Philipp et al., 2004; Basei et al., 2011; Campos et al., 2012; Fischer et al., 2019) and (iii) the infracrustal Camboriú Complex (Basei et al, 2013; Martini et al., 2019a,b). The correlation is proposed by evaluating and comparing the structural record in terms of geometry and kinematics, strain progression and partitioning, timing and deformation conditions in each structural domain. The data are then interpreted and compared with previous models of tectonic evolution of the area, suggesting possible alternative interpretation of the Western Gondwana assembly registered in the northernmost DFB.

2. Geological Setting

2.1 Dom Feliciano Belt Geology

The tectonic evolution and significance of the Dom Feliciano Belt is still a matter of intense debate, illustrated by various models proposed in the past decades (e.g. Fernandes et al., 1992, 1995a, 1995b; Chemale Jr., et al 2012; Philipp et al., 2016). Apart from many differences among these models, the Dom Feliciano Belt is consensually subdivided in four major tectonic domains (Fig. 1) limited by major geological and geophysical lineaments or discontinuities (e.g. Fernandes et al., 1995a,b). The São Gabriel Block, exposed exclusively in the western portion of Rio Grande do Sul state shield area, represents a Neoproterozoic active margin with relicts of an early (oceanic?) arc phase (948 to 850 Ma – Leite et al., 1998; Arena et al., 2016) and a well recognized continental arc (786 – 700 Ma – Saalmann et al., 2011; Arena et al., 2016; Philipp et al., 2018). The Tijucas Fold Belt (Hasui et al., 1975) is a foreland fold-and-thrust belt. It has at least two diachronous volcano-sedimentary sequences, metamorphosed and deformed at *ca.* 650 Ma and shortly after 580 Ma (e.g. Jost and Bitencourt, 1980; Höfig et al., 2017; Battisti et al., 2018), with Paleoproterozoic basement exposed in the inner portions of regional antiforms (Encantadas Complex – Saalmann et al., 2006; Camboriú Complex –Martini et al., 2019a,b). The foreland is covered by late-orogenic volcanic and sedimentary rocks representing infill of narrow grabens (Camaquã Basin – Paim et al., 2014; Itajaí Basin – Guadagnin et al., 2010). Farther to the southeast, the inner portion of Dom Feliciano Belt is represented by batholiths made of polyphase and multi-intrusive, dominantly post-collisional granitic bodies with associated mafic magmatism, the intrusion of which was structurally controlled by the Southern Brazilian Shear Belt (Bitencourt and Nardi, 1993, 2000; Bitencourt, 1996; Florisbal et al., 2012a). Paleoproterozoic (e.g. Gregory et al., 2015), minor Mesoproterozoic (Chemale Jr. et al., 2011) and early-Neoproterozoic rocks (Lenz et al., 2011; Koester et al., 2016; Martil et al., 2017) occur as basement inliers or as regional scale roof pendants (e.g. Encruzilhada Block of Jost and Hartmann, 1984; De Toni, 2019; and the Punta del Este Terrane – Oyhantçabal et al., 2009). Finally, the late Neoproterozoic flysch-type sedimentary rocks of the Rocha Group represent an eastermmost part of the Dom Feiciano Belt exposed exclusively along the eastern coast of Uruguay (Bettucci and Burgueño, 1993).

Both the Tijucas Fold Belt and the batoliths outcrop from southern Uruguay up to the Santa Catarina coast (southern Brazil – Fig. 1b) as a N–S to NE–SW–trending, *ca.* 1200 Km long units limited by some of the major shear zones representing the Southern Brazilian Shear Belt. Basei et al. (2005; 2008) interpreted the batoliths as a magmatic arc accreted to the Tijucas Fold Belt during the Neoproterozoic and proposed that the boundary between these tectonic domains is a suture zone active during collision at *ca.* 600 Ma (Basei et al., 2008). On the other hand, Florisbal et al. (2012a, b, c) demonstrated that synchronous 630 – 610 Ma magmatic intrusions along the Major Gercino Shear Zone and within the Tijucas Fold Belt correlate in terms of their geochemical affinity. Additionally, recent studies in Uruguay (Oriolo et al., 2016) and Rio Grande do Sul (Martil, 2016; Martil et al., 2017; Battisti et al., 2018; De Toni, 2019) demonstrate that both domains record coherent structural evolution.

FIGURE 1

2.2. The Santa Catarina Shield and the study area

The northern portion of the Santa Catarina Shield (Fig. 1c) represents Archean to Paleoproterozoic basement called the Santa Catarina Granulitic Complex or Luis Alves Craton (Hartmann et al., 2000 and references therein), partially covered by the foreland Itajaí Basin (e.g. Guadagnin et al., 2010) in its southern part. The central portion of the shield area is represented by the Tijucas Fold Belt, which is limited against the northern cratonic block and its cover by the dextral transcurrent Itajaí-Perimbó Shear Zone (Silva, 1991), and separated from the southern Florianópolis Batolith by the dextral transcurrent Major Gercino Shear Zone (MGSZ). The latter is the shear zone controlling syntectonic granitic magmatism of the Florianópolis Batholith along its northern boundary (Bitencourt and Nardi, 1993, 2000; Bitencourt, 1996; Florisbal et al., 2012a; Hueck et al., 2018) in post-collisional setting (sensu Liégeois, 1998). The study area covers the boundary between the Tijucas Fold Belt and the Florianópolis Batolith, including the coastal portion of the MGSZ (Fig. 2 and 3).

FIGURE 2

2.2.1 The Tijucas Fold Belt

The geology of the northern Tijucas Fold Belt can be simplified into three major tectonic units which represent its suprastructure, its infrastructure and late-tectonic intrusions (Fig. 3). The Brusque Complex is the supracrustal unit, with metavolcano-sedimentary successions interpreted as rift-related deposits metamorphosed under mid- to upper-greenschist facies conditions, between the chlorite and garnet zones, and locally reaching amphibolite facies conditions (Silva, 1991; Philipp et al., 2004; Basei et al., 2011; Campos et al., 2012). Its lower succession in the southern Brusque Complex, studied by Silva (1991) and Basei et al. (2011), includes an important phase of dominantly mafic, tholeiitic magmatism, interpreted by Campos et al. (2012) as related to the rifting stage of the precursor basin. These authors estimated the local amphibolite-facies conditions at 650 to 660 °C and recognized an early greenschist-facies phase at *ca.* 550°C, both at an arbitrarily fixed pressure of 5 kbar. Recently estimated PT conditions in the garnet-bearing succession of the Brusque Complex by Asvald (2018) point to early garnet growth at 510°C and 4.8 kbar, with peak conditions at 560-570°C and 6-7 kbar. An early deformation phase of thrusting towards NW is recognized in these rocks (Silva, 1991; Philipp et al., 2004; Fischer et al., 2019). Syntectonic peraluminous granites are intrusive along the gently-dipping fabric during the main deformation episode (Philipp and Campos, 2010, Hueck et al., 2016), with ages between 615 ± 4.2 Ma and 599.2 ± 3.8 Ma (LA-ICP-MS and SHRIMP U-Pb zircon – Hueck et al., 2020). These structures are reworked by subvertical, NE-striking, and later NW-striking, brittle-ductile structures (e.g. Philipp et al., 2004).

The basement unit of the Tijucas Fold Belt is the Camboriú Complex (Fig. 2 and 3), which includes ortho- and minor paragneisses of dominantly Archean to Paleoproterozoic protolith ages, with minor Mesoproterozoic mafic intrusions, abundant Neoproterozoic melting features, and the Itapema Granite, interpreted as product of the Camboriú Complex anatexis during Neoproterozoic water-fluxed melting (Hartmann et al., 2003; Rivera et al., 2004; Bitencourt and Nardi, 2004; Basei et al., 2013, Martini et al., 2019a,b). Basei et al. (2013) presented U-Pb SHRIMP ages of 634 ± 24 Ma for a deformed leucosome, and of 637 ± 21 Ma for the Itapema Granite (referred to as the Ponta do Cabeço Diatexite).

Late-tectonic granitic intrusions are abundant in both complexes, and mostly obliterate contacts between them (Fig. 2 and 3). The most voluminous intrusions are the biotite ± hornblende, porphyritic Rio Pequeno Granite (622 ± 15 Ma, 626 ± 7 Ma) and biotite ± muscovite Serra dos Macacos Granite (611 ± 9 Ma), LA-MC-ICP-MS U-Pb zircon ages obtained by Florisbal et al. (2012b). The Rio Pequeno Granite intrusion causes contact metamorphism in the Brusque Complex metasedimentary rocks (Philipp et al., 2004; Fischer et al., 2019) and in the Camboriú Complex xenoliths (Peternell et al., 2010). The deformation of these granites is relatively weak, and therefore they are considered to intrude a low-strain zone relative to the Major Gercino Shear Zone (Peternell et al., 2010; Florisbal et al., 2012b). Local evidence of discrete, sinistral, NNE-striking shear zones was reported by Martini et al. (2015), who studied the syntectonic Corre-Mar Granite

(615 ± 4 Ma –zircon, U-Pb, LA-ICP-MS; Martini et al., 2015), instrusive in the Camboriú Complex along some of these late structures.

2.2.2 The Major Gercino Shear Zone and the Florianópolis Batolith

The Major Gercino Shear Zone is a major structure of dextral, transpressive to transcurrent progressive deformation, which conditioned the syntectonic emplacement of the northernmost granitic and associated mafic intrusions that build the Florianópolis Batolith along its limit with the Tijucas Fold Belt (Bitencourt and Nardi, 1993; Florisbal et al., 2012a; Hueck et al., 2018 among others – Fig. 2 and 3). The basement of the Florianópolis Batolith in the area is the Porto Belo Complex, mostly composed of granitic, granodioritic and tonalitic orthogneiss and foliated tonalite (Bitencourt, 1996; Florisbal et al., 2012a, b). De Toni et al. (2020) reported crystallization age of 798 ± 3.8 Ma (zircon, U-Pb, LA-ICP-MS) for an orthogneiss protolith, whereas Chemale Jr. et al. (2012) presented 649 ± 7 Ma (zircon, U-Pb, LA-ICP-MS) and 646 ± 15 Ma (zircon, U-Pb, ID-TIMS) magmatic ages for the foliated tonalites. The subhorizontal fabric of the Porto Belo Complex rocks was briefly described by Bitencourt and Nardi (1993) and attributed to an unspecified, older tectono-metamorphic event. These authors, however, mentioned that the constant subhorizontal lineation on both gently-dipping and subvertical foliations along the Major Gercino Shear Zone suggests tangential movement compatible with the early stages of transcurrence.

The earlier intrusions along the Major Gercino Shear Zone are the coarse- to very coarse grained, porphyritic Quatro Ilhas Granitoids. These rocks show flat-lying magmatic foliation, sub-parallel to the basement structure (Bitencourt and Nardi, 1993, 2000 – as in Fig. 3). Asymmetric folds show top-to-NW shear sense (Bitencourt, 1996; Florisbal et al., 2012b). Florisbal et al. (2012b) presented magmatic ages of 625 ± 6.5 Ma and 614 ± 4 Ma (zircon, U-Pb, LA-ICP-MS) for the granodioritic and monzogranitic varieties, respectively.

The Quatro Ilhas Granitoids were intruded by the Mariscal Granite (Bitencourt and Nardi, 1993; Bitencourt, 1996) at 609 ± 8 Ma (zircon, U-Pb, LA-ICP-MS – Florisbal et al., 2012a), which was then intruded by the Estaleiro Granitic Complex, consisting mainly of a heterogeneously deformed, porphyritic granodiorite, synplutonic dikes and a network of granitic veins preferentially emplaced in the mylonitic portions (Bitencourt, 1996). This relationship was confirmed by further geochronological studies (Chemale Jr. et al, 2012; Florisbal et al., 2012a; Peruchi, 2016). Peruchi (2016) presented ages of 611.9 ± 1.7 Ma and 611.2 ± 2.7 Ma (zircon, U-Pb, LA-ICP-MS) for the undeformed and mylonitic varieties of the granodiorite, respectively, while Chemale Jr. et al. (2012) report an age of 602 ± 4.2 Ma (zircon, U-Pb, ID-TIMS). Both igneous and mylonitic fabrics of the Mariscal and Estaleiro Granitic Complex were formed under dextral transcurrence (Bitencourt and Nardi, 1993; 2000; Florisbal et al., 2012a).

The Zimbros Intrusive Suite includes the late-transcurrence Zimbros Granite and hypoabissal rocks along the Major Gercino Shear Zone, and the Morro dos Macacos Granite, emplaced to the south, outside the shear zone (Bitencourt, 1996) (Fig. 2 and 3). Bitencourt (1996) described the Zimbros Granite as a late-transcurrence magmatic body that crosscuts the Estaleiro Complex at map scale (Fig. 2), while presenting mostly sheared contacts at outcrop scale, with locally preserved intrusive contacts. The stratigraphic position of this unit was also further confirmed by zircon U-Pb ages reported by Chemale Jr. et al. (2012) as 587 ± 7.5 Ma (LA-ICP-MS) for the Zimbros Granite, 587 ± 8.7 (SHRIMP) for an acid dike, and 588 ± 3.3 (ID-TIMS) for the Morros dos Macacos Granite. Both the Zimbros Granite and the Estaleiro Granodiorite are intrusive in the southeastern portion of the Brusque Complex, where supracrustal rocks present thermal and shearing effects related to the Major Gercino Shear Zone late magmatism (Bitencourt and Nardi, 1993; Philipp et al., 2004).

3. Materials and methods

This study is based mostly on field observations and structural data from key outcrops selected after geological mapping (1:25.000 scale – Bitencourt, 1996; UFRGS, 2000). These data were integrated with petrography, microstructural observation, new and published geothermobarometric and geochronological data, and represent a robust dataset for the three studied structural domains. Eight cross sections were constructed perpendicular to the main structural trend and tectonic boundaries of the area (NE to ENE) and they are integrated in the composite cross section presented in figure 3.

One pseudosection was constructed with the Perple_X 6.7.0 software (Connoly, 2005) and the thermodynamic database of Holland and Powell (1998, revised 2002), based on whole-rock geochemistry obtained using a Rigaku RIX 2000 X-Ray Fluorescence (XRF), in the X-ray Fluorescence Laboratory of Centro de Estudos em Petrologia e Geoquímica (CPGq), Instituto Geosciências (IGEO), at Universidade Federal do Rio Grande do Sul (UFRGS), Brazil. Microprobe analysis was carried out at the Microprobe Laboratory, CPGq/IGEO/UFRGS, using a Cameca SXFive electron microprobe. The analytical conditions were 14.8 keV, 15 nA current, and beam size of 20 µm. Microprobe data were also used for conventional plagioclase-hornblende geothermobarometry (Schmidt, 1992; Holland and Blundy, 1994).

Quartz c-axis fabric data from one key sample are used to complement the kinematic array. EBSD mapping was carried out using a 9.5 µm step-size with a Scanning Electron Microscope (SEM) Zeiss Merlin VP Compact from the SEM Laboratory at the Faculty of Health Sciences of the Arctic University of Norway in Tromsø. The mapped area was 2 cm^2 (2 cm along the mylonitic foliation by 1 cm perpendicular to it). Post-processing of SEM data was made with AzTEC software. All thin sections analysed in SEM, with microprobe or EBSD, were carbon coated.

4. The Porto Belo – Camboriú cross section

Data from each individual cross-sections which compose figure 3 (locations indicated in Fig. 2) will be presented separately, organized in three major structural domains, from southeast to northwest: i) the Florianópolis Batholith, including the Major Gercino Shear Zone; ii) the suprastructure, and iii) the infrastructure of the Tijucas Fold Belt.

FIGURE 3

4.1 Florianópolis Batolith and the Major Gercino Shear Zone

The cross-section A–A' (Fig. 2 and 3) starts in the Morro dos Macacos Granite, which was described by Bitencourt and Nardi (1993) as an isolated intrusion without observable contact relations. The granite is dominantly isotropic, although magmatic foliation and discrete shear zones are locally developed. Roof pendants of the Porto Belo Complex are exposed in its southwestern portion. The northern limit of this section is placed in the Mariscal Granite, which marks the inferred southeastern boundary of the Major Gercino Shear Zone. The Mariscal Granite is commonly found as small intrusions in the Quatro Ilhas Granite (Bitencourt and Nardi, 1993, as depicted in section B – B', Fig. 3) and is a fine- to medium-grained rock recording dextral transcurrence both during early high-T and late low-T deformation along mostly subvertical shear zones (Bitencourt and Nardi, 1993, 2000; Bitencourt, 1996; Florisbal et al., 2012a).

The cross section from Ponta de Fora to Ponta da Garoupa (B – B' section, Fig. 2 and 3) exposes interleaving of the Quatro Ilhas Granitoids with the Porto Belo Complex along its original flat-lying foliation at map and outcrop scale. The Quatro Ilhas Granitoids are the earliest reported intrusions along the Major Gercino Shear Zone (Bitencourt and Nardi, 1993; 2000; Bitencourt, 1996; Florisbal et al., 2012a). Leucogranitic and mafic-rich varieties of this porphyritic granite are interleaved along its magmatic foliation (Fig. 4a and b), mostly defined by the alignment of subhedral K-feldspar phenocrysts (0.5 to 5 cm) and matrix minerals, mainly biotite. A mylonitic foliation is heterogeneously developed parallel to the magmatic one (Fig. 4a). The foliation dips mostly to SE at low to high angles due to asymmetric folding (Fig. 4a). The asymmetric folding leads to a half-girdle pattern of the pole to foliation distribution in the stereoplot (Fig. 4c). The folding brings the foliation to subvertical position, where strike-slip shear zones may develop (Fig. 4d). Mineral lineation is defined by preferred orientation of phenocrysts in the foliation plane, and a stretching lineation is developed parallel to it due to recrystallization of both K-feldspar phenocrysts and quartz-feldspathic matrix. Both mineral and stretching lineations are subhorizontal and parallel to the fold axes (Fig. 4c).

FIGURE 4

Fold profiles show folded zones of aligned K-feldspar phenocrysts with well-preserved subhedral igneous shape. These sections are ideal to observe the shortening and top-to-NW thrusting components of the transpressional deformation recorded in these rocks (Fig. 4a and b). On the other hand, subhorizontal surfaces record its dextral transcurrent component, with well developed S-C-C' structures and mostly asymmetric porphyroclasts (Fig. 4d).

The Porto Belo Complex main outcrop in this section is at Ponta das Bombas (Fig. 3 and Fig. 5a, b), which features the inner portion of a major antiformal structure build up by the Porto Belo Complex rocks and flanked by the Quatro Ilhas Granitoids. Most of the rocks in the area are granites to tonalities in composition, with preserved magmatic texture, containing gneiss lenses or tabular bodies (maximum 1.5 m width and up to 10 m long, Fig. 5c, d and e). Igneous rocks are medium- to fine-grained hypidiomorphic, with different degrees of deformation. They apparently represent a continuous variation between foliated leucosyenogranites with sparse biotite aggregates and schlieren (Fig. 6a and b), through foliated or banded monzogranites with biotite ± muscovite (Fig. 6c) to biotite ± hornblende granodiorites and tonalites (Fig. 5e and Fig. 6d), with either irregular, abrupt, gradual or diffuse contacts (Fig. 5d and e). The banded varieties show discontinuous banding given by biotite-rich, mm-wide bands or lenses, and by variations in grainsize (medium to fine, locally pegmatitic) and mafic mineral content. Elongate gneissic lenses enhance the banding (Fig. 5d) and contribute to its development by mechanical disaggregation of their margins by magmatic flow. Their disruption eventually leads to the formation of schlieren along the foliation of granitic rocks (e.g. lower portion/first plane of Fig. 5b and Fig. 6a and b). The gneisses are predominantly biotite (± hornblende) orthogneisses with quartz-dioritic, tonalitic and granodioritic compositions (Fig. 6e and f). Calc-silicate paragneisses (with up to 90% diopside) are restrictd to one specific level where they are boudinaged into round, dm-wide greenish fragments (Fig. 7a). They are found in the southern portion of the Ponta das Bombas outcrop, which represents the upper structural level of the Porto Belo Complex sequence, dipping to SE.

FIGURE 5

FIGURE 6

Igneous and metamorphic rocks are here described as intimately related in a migmatitic association. Some of the orthogneiss fragments show cm-size melt patches containing euhedral titanite (up to 3 mm long) immersed in allotriomorphic quartz-feldspathic matrix, which is coarser grained than the surrounding gneiss. These structures (Fig. 6e and 7b) are similar to those described by Martini et al. (2019a, b) in the Camboriú Complex migmatites. Melt mobility seems to have been efficient along the main banding of metatexites, leading to coalescence of mm- to cm-wide veins that crosscut the main banding (Fig. 5c, 5e, 7b). Oblique veins also coalesce in wider leucogranitic ones rooted in the banded rock (Fig. 5d), or in wider, structurally independent diatexitic levels that may carry fragments of source rocks (Fig. 5e and 7a).

The structural framework of the Porto Belo Complex migmatites at Ponta das Bombas is shown in Fig. 7c. Poles to foliation are arranged in a half girdle with NE-striking, subhorizontal to subvertical planes of tight to isoclinal folds. The distribution single maximum represents foliation planes that dip to SE at moderate angle and are subparallel to fold axial planes. Mineral and stretching lineations display a half-girdle in the SW quadrant and plunge at low- to medium-angle towards SW to S. Orientation of axial planes is very similar to the foliation distribution, while fold axes are similar to lineation distribution, but more spread. The spreading of fold axes may be due to the presence of convolute (Fig. 7e) and disharmonic (Fig. 7f) folds, possibly related to locally high melt mobility.

FIGURE 7

Contact relations between the Porto Belo Complex migmatites and the Quatro Ilhas Granitoids are best observed in the southern portion of Ponta das Bombas. In this area, the Quatro Ilhas Granitoids overly the migmatitic rocks (Fig. 3 and 8a) and mutual crosscuting relations are observed. Leucogranitic veins rooted in the melt-rich metatexite bands cross the contact and the magmatic foliation of the Quatro Ilhas Granitoids (Fig. 8b and c). The granite surrounds slices of metatexites in the contact vicinity, with foliation parallel to the contact, disrupting and probably assimilating the metatexite during magmatic flow (Fig. 8d).

FIGURE 8

It is worth to note that the NNW – SSE sections represent fold profile planes that are oblique to perpendicular to lineations, and expose the best kinematic indicators seen at the outcrop, including abundant gneissic fragments as asymmetric sigma-shaped clasts (Fig. 7a and 7d), and high-strain zones where the axial planes evolve into a transposition foliation, so that duplex structures are formed (Fig. 7f) at outcrop scale. All observed kinematic indicators along NNW – SSE subvertical exposures express an apparent top-to-NNW thrusting component, while kinematic indicators along subhorizontal planes indicate a dextral component. The evidence points to a coherent kinematic framework of oblique, top-to-NNW dextral transpression, very similar to the one observed within the Quatro Ilhas Granitoids.

Porphyroclasts in deformed granitoids (Fig. 6d and 8d) and orthogneisses (Fig. 6f), and sheared melt pockets found in the latter (Fig. 6e), are consistent with this kinematics. Feldspar porphyroclasts are mostly rounded or lenticular relict crystals with mica or quartz shaping the asymmetric recrystallization tails (e.g. Fig. 6a, b and c), which is indicative of subordinate feldspar recrystallization processes. The feldspar porphyroclasts are often fractured, with some of these fractures filled by subhedral to anhedral quartz-feldspathic matrix (± biotite), which is suggestive of deformation in the presence of melt (inset of Fig. 6c). Subhedral phenocrysts are also common as preserved igneous texture (Fig. 6c and d). On the other hand, orthogneisses present both high temperature and lower temperature deformation features, as for example recrystallized plagioclase in the granoblastic matrix, and kinked plagioclase porphyroclasts marginally replaced by fine-grained mica (Fig. 6f).

The beach outcrops represent lower structural levels relative to the Ponta das Bombas section. The observed features in these places are similar to those described above, apart from discrete dextral transcurrent shear zones that become more important, and some of them assist the emplacement of the Mariscal Granite intrusions (Fig. 3).

Farther north (C-C' in Fig. 2 and 3), the Estaleiro Granitic Complex and the Zimbros Granite exhibit NE-striking dextral strike-slip tectonics (stereonet D in figure 03) recorded by both magmatic and mylonitic fabrics (Bitencourt and Nardi, 1993; Bitencourt, 1996).

4.2 Tijucas Fold Belt suprastructure – the Brusque Complex

The contact between the Estaleiro Granodiorite and metapelitic schists of the Brusque Complex (D-D' in Fig. 2 and 3) was described by Silva (1991) and Bitencourt (1996) in the Sertão de Santa Luzia region (Fig. 2). At this locality, the authors describe a progression from undeformed to mylonitic Estaleiro Granodiorite, and a strong mylonitic foliation oriented (060°/65°NW) in the Brusque Complex rocks to the northwest, that transposes previous subhorizontal contacts between quartzites and garnet-muscovite schists. Bitencourt (1996) interpreted the latter to be the Estaleiro Granitic Complex country rocks at the NW boundary of the Major Gercino Shear Zone. According to that author, the supracrustal rocks were intruded by the syntectonic Estaleiro Granodiorite after the Brusque Complex main metamorphism and deformation event.

The approximately 4 km long E-E' section along the 340° – 160° trend (location in Fig. 2) crosses the metavolcano-sedimentary pile of the south Brusque Complex (Fig. 9a; see also Campos et al., 2012). From the whole section, one outcrop was chosen for detailed observations due to its convenient orientation perpendicular to the structural trend and continuous exposure (Fig. 9b). The exposed sequence comprises metabasalts, calc-silicate rocks, qtz + bt schists, minor ultramafic rocks and early- to late-tectonic leucogranite injections, mostly as cm- to m-thick bodies at low-angle or along the main foliation, but also as larger bodies crossing the fabric at high-angle (Fig. 9; see Philipp and Campos, 2010; Hueck et al., 2016, 2020). The main foliation (S_x) is defined at outcrop scale by interleaving of the above-mentioned rock types. At hand-sample scale, it is characterized by the alignment of metamorphic minerals such as amphibole and feldspar or by alternating biotite-rich and quartz-rich bands. The schists show intrafolial folds with partially transposed earlier foliation (S_{x-1} parallel to S_x – not shown) marked mainly by trails of opaque minerals along biotite aggregates. The main foliation strikes NE-SW and dips gently to NW (Fig. 9c), with poles to foliation forming an incomplete girdle due to asymmetric recumbent folds (see Fig. 9d). Along this cross-section, and independent of observation scale, fold asymmetry is strong and suggestive of top-to-NW shear sense. Because they are tight folds, their axial planes tend to plot with the pole to foliation distribution. Fold axes spread in the SW and NE quadrants, near foliation/axial plane strike. Mineral and stretching lineations, marked by amphibole crystals and quartz aggregates, respectively, are subparallel and consistently concentrated near the dip direction, plunging at shallow angle towards NW. The variation of fold axis orientation between fold axis maximum and stretching direction (Fig. 9c) also points to fold shearing during progressive deformation. Apart from fold asymmetry, kinematic indicators are virtually absent.

FIGURE 9

Deformation of the heterogeneous rock pile with an apparently high rheological contrast between layers is exemplified by disharmonic folding of different compositional layers, commonly showing thickened fold hinges and thinned or boudinaged limbs (e.g. Figs. 9d and 10a). Relatively soft calc-silicate schists show highly asymmetric fold pattern, given by SE long limbs and NW short, inverted limbs (Fig. 10c). Fold asymmetry along this section consistently shows top-to-NW vergence (Fig. 10b and 10c).

Discrete shear bands of opposite shear-sense are locally present in quartz-biotite schists (Fig. 10b) and epidote-rich calc-silicate rocks (Fig.10d). Quartz-biotite schists have cm-spaced planar structures which develop stretching preferentially subparallel or along the long limbs of cm-size asymmetric folds. These structures are marked mainly by the thinned out or disrupted quartz-rich layers, but also by obliquely oriented, discontinuous flanking structures (Fig. 10b) which segment the rock into asymmetric foliation boudins. Some of these structures are filled with quartz-feldspathic material (upper-left portion of Fig. 10b), which suggests their dilational character.

In epidote-rich calc-silicate rocks, reworking of the main foliation gives rise to fine-grained, discrete, anastomosed array of mylonitic foliation (S_{x+1} in Fig. 10d). This younger mylonitic fabric takes advantage of the previous structure, but mostly represents a transposition foliation sub-parallel to axial planes of folds. Hinge zones are domains of preserved S_x which form pods surrounded by high-strain zones. An apparent strain gradient is observed towards the center of these structures, where grain size is minimum and elongation is maximum. Pod asymmetry and deflection of folded metamorphic foliation towards high-strain zones of S_{x+1} indicates a top-to-SE movement along these late structures, which thus suggest reactivation of gently-dipping planar structures at distinct PT-fluid and/or higher-strain conditions.

Randomly-oriented, post-kinematic porphyroblasts (andalusite?), pseudomorphically replaced by white mica, are locally found along the profile (Fig. 10e). Thermal effects like this are in agreement with observations made by Philipp et al. (2004) along the contacts between Brusque and Camboriú complexes.

FIGURE 10

4.3 Tijucas Fold Belt infrastructure – the Camboriú Complex

The contact between the supra- and infracrustal units of the Tijucas Belt is exposed in the area north of the Serra da Miséria ridge (D-D' in Fig. 2 and 3), which features mylonitic leucogranites considered to be part of the Camboriú Complex (Hartmann et al., 2003; Bitencourt and Nardi, 2004; Rivera et al., 2004). This mylonite, in contrast with the rest of the Camboriú Complex rocks, has markedly well developed linear fabric, and locally forms L-tectonites. To the north of this ridge there is a ca. 1 km long, approximately EW trending lens of Brusque Complex rocks in contact with the granitic mylonites that roughly mark the boundary of the Camboriú Complex (Fig. 2). The boundary between the complexes is exposed at outcrop scale along the valley (Fig. 11a), where the foliations of both are concordant and parallel to the contact. The distribution of poles to foliation from both units (Fig. 11b) suggests a coherent girdle, with a single maximum dipping at moderate angles towards SSW, parallel to the observed contact (fig. 11a), which suggests that both units were folded together.

FIGURE 11

Camboriú Complex mylonite stretching lineation and Brusque Complex amphibole alignment and stretching lineation are mostly subhorizontal and also roughly concordant, with ENE-plunging maximum. Spreading of orientations may be due to late folding effects.

The intrusive relationship between the Camboriú Complex mylonitic granite and the Brusque Complex amphibolite is locally observed (Fig. 11a and c) as deformed apophyses of the first that crosscut the mylonitic foliation of the amphibolites at low-angle. In the amphibolite, apparent increase of strain towards the contact leads to the development of more pervasive mylonitic foliation. Disrupted quartz veins crosscut both units near the contact. Some of them are transposed along the mylonitic foliation of the amphibolites and register oblique shearing with dextral (Fig. 11d) and normal, top-to-SW, components (Fig. 11e).

The L > S fabric of the Camboriú Complex mylonitic granite was evaluated in terms of observed deformation mechanism and kinematics through petrography and EBSD. The rock has up to 50% quartz, which forms up to 3 mm-long porphyroclasts with undulose extinction and oblique subgrain boundaries, and dynamically recrystallized, fine-grained matrix. K-feldspar porphyroclasts (ca. 2 mm) show extensional fractures filled by quartz. Mica flakes are rare.

Quartz c-axis orientation data from the same sample were processed in two different grain-size groups with arbitrary threshold at 100 µm, according to a change in histogram of grain-size distribution (not shown). C-axis distribution for quartz crystals larger than 100 µm form an asymmetric, well-defined single girdle, or an ill-defined cross girdle (Fig. 11g). Quartz crystals smaller than 100 µm have c-axes distributed in a similar but better defined cross girdle (Fig. 11h). The general orientation is much more random when compared with the fabric of the larger grains, as shown by the maximum density in contoured diagram.

Microstructures as oblique quartz porphyroclast long-axis, asymmetry of lens-like fine-grained quartz aggregates or mica lenses contouring porphyroclasts, and more rarely seen mica fish are indicative of an oblique, dextral, top-to-WSW movement along the mylonitic fabric (Fig. 11f). The apparent dextral asymmetry (top-to-SW) is confirmed by quartz c-axis distribution (Fig. 11g and h).

The Brusque-Camboriú contact is reworked by a NE – SW fault system (Fig. 3), possibly related to a late reactivation of the Major Gercino Shear Zone (Hueck et al., 2018). The effects of later movements were observed at the outcrop as fault-controlled quartz veins and fracture zones (Fig. 11a). Fault-related rocks are amphibolitic breccia and mylonitic quartz (Fig. 11i) or cataclastic juxtaposition of units along shear fractures (Fig. 11j).

Farther to the north (F-F' in Fig. 2 and 3), the Itapema Granite was described in detail by Rivera et al. (2004) and Bitencourt and Nardi (2004) as a hornblende-biotite granodiorite to monzogranite with large volume of xenoliths (ca. 20 fragments/m^2) organized along a strongly developed, subhorizontal magmatic flow banding (Fig. 12a). The banding is given by different proportions of oriented mafic minerals, disrupted xenoliths, schlieren and pegmatites injected parallel to the main foliation (Fig. 12b). However, no lineation is found. Apparent kinematic indicators, as asymmetric xenoliths, are observed along NW – SE sections, but they are not conclusive in terms of shear sense.

FIGURE 12

The Camboriú Complex (G-G' and H-H' in Fig. 2 and 3) main petrological and structural features were recently described by Martini et al. (2019a, b) and the main results and interpretations are summarized as follows. The metamorphic rocks are mostly orthogneisses and amphibolites, with minor paragneiss of pelitic and calc-silicate composition. The main structure is an originally subhorizontal metamorphic banding that rarely bears a stretching lineation and is enhanced by partial melting features (Fig. 12c, d). A possibly older folding phase was recognized locally as transposed, intrafolial folds, whose significance remains unknown. The main banding is affected by open to tight upright folds of NE–SW to N-S, subhorizontal axes (Fig. 12d), developed during partial melting, as suggested by syn-magmatic shear bands along limbs and axial planes (Fig. 12e). Opposite limbs of the same antiform may act as conjugate shear bands with opposite shear sense, causing collapse of limbs and synforms, while antiforms are extruded (Fig. 12f). These channels occasionally coalesce to generate melt extraction dikes which are interpreted as feeders of the Itapema Granite magmatic chamber (Martini et al., 2019a, b).

5 Geothermobarometry

5.1 Porto Belo Complex crystallization conditions

One sample from a diatexitic hornblende-biotite tonalite with epidote and titanite was selected for geotermobarometry. The rock is foliated and presents well-preserved igneous textures, as exemplified by subhedral plagioclase and hornblende crystals (Fig. 6d).

Nine representative hornblende – plagioclase pairs were selected based on apparent equilibrium conditions (table 1 and 2), as exemplified by direct contact relations and preserved igneous shapes. The analysed spots were preferentially positioned close to shared boundaries. The results from each pair are presented in Table 3. The estimated conditions range from 676 to 722 °C, and 3.7 to 4.8 kbar. The average conditions are 707 °C and 4.3 kbar.

TABLE 1

TABLE 2

TABLE 3

5.2 Camboriú Complex metamorphism and melting conditions

A migmatitic sillimanite-garnet-biotite gneiss (Fig. 13a) was selected for pseudosection modelling. The rock has *ca*. 5% garnet porphyroblasts (up to 1.5 cm in diameter) embedded in a sillimanite-bearing, biotite-rich matrix which also contains ilmenite as accessory phase. The rock also presents irregular pockets and lenses of granitic leucosome along the banding. Subhedral garnet is present in the leucosome, which suggests its equilibrium during partial melting at peak metamorphic conditions (Fig. 13b). The metapelite exhibits rare relics of kyanite, partially replaced by sillimanite (Fig. 13c), which suggests prograde metamorphic history and/or exhumation from deeper to shallower levels.

FIGURE 13

The pseudosection for this rock (Fig. 14) presents the observed assemblage biotite + garnet + sillimanite + plagioclase + quartz + ilmenite ± melt ± water in its central portion. The fields are limited from the lower pressure fields by the cordierite-out curve and from the higher pressure fields by the kyanite – sillimanite reaction boundary. The melt-in curve position should be taken with caution and is not considered a boundary to the estimated conditions. Since it is visible from the hand-sample that the melt was somehow mobile, the system composition may be impoverished from the melt loss, and the melt-in curve will be shifted to higher temperatures.

Representative mineral chemistry of biotite and garnet is presented in table 4. Thirteen biotite grains were analysed in the metamorphic matrix. The compositional range is expressed by XMg (Mg/[Mg+Fe]) values from 0.31 to 0.37, with a median and average of 0.34. The isopleths for the observed range of XMg values for biotite are widely spaced and cover most of the stability fields representing the observed assemblage. Since these isopleths do not help to constrain the PT conditions, they were not plotted in the figure 14.

From three analysed garnet porphyroblasts, just one of them presented core – rim zonation, while the other two presented nearly constant composition independent of position. In the weakly zoned garnet crystal, core presents slightly higher content of grossular and lower almandine component ($Alm_{74-75}Py_{12}Sp_7Gro_{7-8}$) if compared with rim ($Alm_{78}Py_{11}Sp_8Gro_3$ – see Fig. 13b).

TABLE 4

Isopleths for grossular (up to 3%), pyrope (11 – 12%) and spessartine (6 – 7%) define a narrow area overlapping the stability fields of the observed mineral assemblage, which is above the cordierite-out limit and crosses the melt-in curve. This area is equivalent to 665 – 705°C and 4.4 to 5.3 kbar, which is interpreted as the conditions of residual melanosome reequilibration after some melt loss (Fig. 14). Almandine isopleths were not plotted because they are widely-spaced and do not help to constrain the PT conditions. The upper limit of temperature and the pressure range are compatible with the solidus conditions of the Itapema Granite estimated by Rivera et al. (2004) at 700 °C and 4–4.5 kbar, and within the range of the in situ leucosome crystallization conditions of 700 – 750° and 3.4 – 4.2 kbar by Martini (2019). Additionally, the estimated conditions for the Camboriú Complex migmatitization are also comparable with the crystallization conditions of the Porto Belo Complex diatexite.

6. Discussion

The following discussion is organized in terms of the three major structural domains - Major Gercino Shear Zone, suprastructure and infrastructure of the Tijucas Fold Belt. The deformation history of each domain is discussed and followed by kinematic correlation between domains in order to consider the combined effects of strain partitioning in space and progressive deformation in time, and its implications for the evolution of Dom Feliciano Belt.

6.1 Oblique transpression recorded in the Major Gercino Shear Zone progressive deformation

Structural features of the Porto Belo Complex indicate transpressive deformation composed of dextral transcurrence and NNW-directed thrusting. The vorticity-normal section of the system is estimated as 340° – 160° subvertical sections (e.g. Fig. 5a, b and 6d, f). It is the best fit great circle to the distribution girdle of poles to foliation (Fig. 7c) as pointed out by Fernandez and Díaz-Azpiroz (2009), and also considered to be the plane of maximum fabric asymmetry (Goodwin and Williams, 1996). A lineation half-girdle formed by orientations ranging from nearly dip-direction to nearly strike-parallel, and plunging to opposite senses (Fig. 7c) also suggests an oblique, triclinic character of the transpressional deformation (Fernandez and Díaz-

Azpiroz, 2009). According to the same authors, the triclinic character may be a consequence of non-vertical shear zone or due to the existence of an angle between extrusion direction and shear direction.

The estimate of crystallization conditions from a diatexitic tonalite is ca. 710°C and 4.5 kbar. Partial melting features are conditioned by these structures, which apart from asymmetry resemble the same partial melting processes described by Martini et al. (2019a, b) in the Camboriú Complex. The presence of titanite and hornblende as perithetic phases, and locally of magnetite, suggests water-fluxed melting processes (Sawyer, 2008, Weinberg and Hasalova, 2015).

The age recently reported by De Toni et al. (2020) for the Porto Belo orthogneiss indicates Tonian (798 ± 4 Ma) protolith. This justifies the re-interpretation of ca. 650 Ma age value for foliated tonalites from the same unit (Chemale Jr. et al., 2012), as a good approximation of the partial melting event coeval with the main thrusting towards NNW (as also argued by Hueck et al., 2018).

Subhorizontal structures attributed to an early deformational phase are also observed within the Quatro Ilhas Granitoids (624 – 615 Ma, Florisbal et al., 2012a), with magmatic/mylonitic foliation gently-dipping to the SE, asymmetrically folded and indicating top-to-NW thrust component (Fig. 4a and b). The gently-dipping foliation, together with strike-parallel mineral and stretching lineations, are characteristic of tangential regimes.

Additionally, asymmetrical folds in the Quatro Ilhas Granitoids are more open if compared with the ones observed in the Porto Belo Complex rocks (Fig. 4 and Fig. 7, respectively). These observations are taken together as evidence of the transitional character of the tangential deformation registered by the Quatro Ilhas Granitoids, as it succeeds the climax of the thrust-dominated transpressional phase recorded in the Porto Belo Complex and preceeds transcurrence-dominated transpression recorded by later intrusions. The mutual crosscutting relationships described between the Quatro Ilhas Granitoids and injections rootedin the Porto Belo Complex migmatites (Fig. 8) also contribute to the understanding of the progressive deformational history recorded by the above-mentioned units.

Dextral strike-slip tectonics along the Major Gercino Shear Zone is well recorded by the Mariscal Granite (614 ± 27 Ma) and definitely established during emplacement of the Estaleiro Granitic Complex (between

611.9 ± 1.7 Ma and 602 ± 4.2 Ma). Both units record parallel magmatic fabric and solid-state deformation heterogeneously distributed in low- and high-strain zones (Fig. 2 and 3; Bitencourt, 1996; Florisbal et al., 2012a).

As the later intrusions along the Major Gercino Shear Zone, the rocks of the Zimbros Intrusive Suite show transcurrence-related magmatic fabrics and minor solid-state deformation along discrete, dextral shear bands (Bitencourt, 1996). Chilled margins against the host rocks, and the hypoabissal rock association indicate the shallow-level condition of these intrusions. As pointed out by Bitencourt (1996), the oblique character of the Major Gercino Shear Zone dextral transcurrence is increasingly important in its late structures, given by stretching lineations that plunge up to 30° SW, as recorded in the Zimbros Intrusive Suite. This later, oblique component, together with dextral shear sense, is responsible for an uplift of the NW block (Tijucas Fold Belt) relative to the SE one (Florianópolis Batolith) (Fig. 1 and 2).

6.2 Camboriú Complex symmetrical folding and exhumation path

The Camboriú Complex fabric is mainly planar (S_b), with rare lineation and no significant asymmetric features. It was originally subhorizontal or gently-dipping, and symmetrical, upright folds with NE – SW subhorizontal axes record NW-SE shortening. The syn-magmatic shear bands of opposite shear sense along limbs of outcrop-scale folds suggest apparent extrusion of the Camboriú Complex hinge zones (Fig. 12f), similar to situations found in other migmatitic terranes (e.g. Sawyer, 2008; Weinberg et al., 2013).

The axial planes locally evolve into a discrete transposition cleavage marked by syn-magmatic shear bands which served as migration paths for crustal melts. These features, together with a general absence of lineation, are interpreted as indication of important pure shear component during progressive deformation of the Camboriú Complex (Martini et al., 2019b). The structural control of melt migration along syn-magmatic shear zones and dikes related to symmetrical folds points to interplay of melting and deformational processes, which have assisted exhumation of the complex.

The exhumation path of the Camboriú Complex can be traced from integrated PT estimates for its various rock types, from 4.5 – 5.5 kbar to 3.5 kbar, as shown in figure 15 (estimates from other structural domains also shown for comparison). Additionally, relict kyanite found in metapelite (Fig. 13c) is considered as a marker for the PT conditions that pre-dated the modelled equilibrium of its stable assemblage. These conditions may have been either of higher pressure or lower temperature, or a combination of both.

FIGURE 15

Despite the errors, the Camboriú Complex ages (637 ± 21 Ma for the Itapema Granite, and 634 ± 24 Ma for the neosome) are in agreement with field relationships and magmatic ages reported for the Rio Pequeno Granite (622 ± 15 Ma; 626±7 Ma) and Serra dos Macacos Granite (611 ± 9 Ma), both emplaced along the contacts of the Camboriú and Brusque complexes (Fig. 2 and 3). The Camboriú Complex exhumation path tracked by PT data is considered to reflect its tectonic juxtaposition to the Brusque Complex suprastructure before or during the Rio Pequeno Granite emplacement.

6.3 Brusque Complex as the foreland fold and thrust belt: thrusting followed by extension?

At the coastal section (E-E’ - Fig. 9), the Brusque Complex subhorizontal foliation (S_x) dips to NW and contains a highly oblique mineral/stretching lineation (L_x). Despite the absence of other kinematic indicators, the common presence of asymmetric, nearly recumbent folds over S_X with predominantly NE-trending axes (Fig.9c and d) is compatible with a NW-directed thrusting event. The NW vergence of asymmetrical folds related to an early deformation phase is consistently argued for by numerous authors in different portions of the Brusque Complex (e.g. Silva, 1991; Philipp et al., 2004; Basei et al., 2011; Fischer et al., 2019).

The increase of wave-length to amplitude ratio from SE to NW along the same axial plane of asymmetric folds of carbonate-rich calc-silicate layers (Fig. 10c) is interpreted as due to strain propagation from SE towards NW. Therefore, fold propagation towards NW is achieved by amplification of an irregularity restricted to that soft layer, since it does not affect the layer above. This rheological boundary may thus have acted as a detachment zone at the outcrop scale.

Discrete, antithetic shear bands (S_{x+1}) developed along fold long limbs indicate extensional reactivation along flanking structures, with collapse of the SE block relative to the NW one (Fig. 10b and d). This interpretation is in agreement with the oblique dextral plus normal shear observed at the Brusque-Camboriú contact in the Serra da Miséria area (Fig. 2 and 3), as well as with the later increments of dextral strike-slip along the Major Gercino Shear Zone. Extensional reactivation of thrust nappe stacks is well recognized, e.g. in the Caledonian nappes of Norway, where it is considered as intimately related to exhumation processes in post-collisional settings (Fossen and Rykkelid, 1992; Andersen, 1998).

An alternative interpretation of such structures may consider folding as a direct result of extension, with asymmetry developed during back-rotation between two high-strain zones of normal movement (Fig. 10b and d), as argued by Harris et al. (2002). The consistent asymmetry exhibited by all observed folds at multiples scales along the cross-section (Fig. 9 and 10), mostly not limited by antithetic-looking shear bands, does not favour this hypothesis.

Local contact metamorphism affecting the Brusque rocks (Fig. 10e) is in agreement with observations near the contacts with the Camboriú Complex (Philipp et al., 2004) and younger granites (Philipp et al., 2004; Peternell et al., 2010; Fischer et al., 2019). It is also noteworthy that amphibolite-facies conditions for this part of the complex are restricted to the Itapema area (Fig. 2), where it is in contact with the Camboriú Complex (Philipp et al., 2004; Campos et al., 2012), in contrast with the regional greenchist facies conditions reported elsewhere in the eastern part of the Brusque Complex (Silva, 1991; Philipp et al., 2004; Basei et al., 2011; Campos et al., 2012; Asvald, 2018; Fischer et al., 2019).

Altogether, observations suggest that the regional greenschist facies, top-to-NW thrusting event has affected the studied coastal section (as argued by Campos et al., 2012), but it also indicates that these rocks have locally reached amphibolite facies conditions by progressive exhumation of the underlying Camboriú Complex migmatites due to regional transpression. This has lead to progressive unroofing of the Brusque

Complex, with development of discrete antithetic shear bands (Fig. 10b and d) and detachments (Fig. 10c) simultaneous to static neocrystallization of low-pressure metamorphic minerals along relatively undeformed bands (Fig. 10e). On the other hand, structures and contact relations between these complexes (Fig. 11) suggest that the Brusque Complex amphibolite facies fabric developed concordant to the mylonitic fabric of Camboriú Complex, and that the amount of finite strain increases towards the contact. Tectonic juxtaposition of the complexes resulted from dextral-normal shearing along a detachment zone at their boundary.

The depth of such event should be equal to, or shallower than, that determined for the Camboriú Complex neosome and Itapema Granite crystallization (3.4 – 4.5 kbar). An attempt was made at estimating pressure conditions from an amphibolite of the Brusque Complex. By using the method proposed by Molina et al. (2015), with hornblende – plagioclase microprobe data taken from Campos et al. (2012), the calculation resulted in a pressure estimate of 3 to 3.2 kbar (see electronic appendix and Fig. 15). Considering the thermal effect of the Camboriú Complex migmatites over the Brusque Complex, and the intrusive relations observed at the contact (Fig. 11a and c), their juxtaposition must have taken place approximately at the time of neosome and Itapema Granite crystallization (ca. 635 Ma). It must also be older than the Rio Pequeno Granite intrusion (ca. 625 Ma), since the latter causes thermal effects over both complexes. The PT-paths (Fig. 15), together with quartz c-axis orientation data (Fig. 11g and h), are interpreted in terms of tectonic juxtaposition resulting from progressive deformation under retrograde conditions and relatively constant strain ellipsoid orientation, with oblique, dextral-normal, top-to-SW shear sense. Fault-related rocks near the contact (Fig. 11i and j) suggest further reactivation of high-T structures under lower temperatures.

6.4 Kinematic correlation and contrasting PT paths

6.4.1 Oblique collision

Each structural domain records the thrusting event at different crustal level and corresponding PT conditions (Fig. 15 and 16a). This event is considered to have occurred at 650 – 645 Ma (Fig. 16a), as recorded by metamorphism and associated partial melting in the Porto Belo Complex. However, a slightly diachronous evolution during strain propagation through the different domains and structural levels cannot be ruled out.

A characteristic triclinic transpressional pattern (as defined by Jones et al., 2004; Fernández and Diaz-Azpiroz, 2009; Fernández et al., 2013; and references therein) is recorded in the structures of the Porto Belo Complex, with a combination of NNW-directed thrusting and dextral transcurrence. Hornblende – plagioclase geothermobarometry of a tonalitic diatexite points to crystallization conditions (705 – 710°C, 4.5 kbar) that are very similar those of the Itapema Granite, equivalent to 13 – 15 km of depth. Observations also suggest that both the Porto Belo and Camboriú complexes have undergone water-fluxed partial melting.

Despite the general absence of lineations on the Camboriú Complex subhorizontal banding, asymmetric structures observed in subvertical sections oriented 340° to 320°, especially along the Itapema Granite magmatic banding, indicate both top-to-NW and top-to-SE shear senses. Such inconclusive vergence is suggestive of pure shear, but may also be attributed to deformation partitioning preferentially into the softer, partly crystallized magma. On the other hand, the presence of intrafolial folds observed along the main banding of Camboriú Complex migmatites suggests deformation of a pre-existing foliation. Peak metamorphic conditions are estimated at 700 – 750°C and 4.5 – 5.5 kbar, but kyanite relicts point to an even deeper origin for the Camboriú Complex. The age of the Camboriú Complex main tectono-thermal event is recorded at ca. 635 Ma (Fig. 16b).

The relative younging of ages, from 650-645 Ma melting in the Porto Belo Complex to ca. 635 Ma in the Camboriú Complex, suggests strain propagation (Fig. 16b), starting from hinterland (SE) towards the foreland (NW), which is in agreement with top-to-NNW vergence of the oblique collision recorded in different domains.

In the Brusque Complex, top-to-NW thrusting is mainly recorded by asymmetrical fold vergence (Fig. 9 and 10), as also reported from other parts of the complex (Silva, 1991; Philipp et al., 2004; de Campos et al., 2012; Fischer et al., 2019). Thrusting and contractional conditions are kinematically coherent with those observed in other studied units, and they are interpreted to be linked, both in time and genesis, to the flat-lying fabrics found in the other structural domains. Additionally, the ca. 645 Ma oblique collision hereby described for the northern Dom Feliciano Belt is correlated with similar tectonic evolution recognized by many authors in the central and southern Dom Feliciano Belt (e.g. Oyhantçabal et al., 2009; Lenz et al., 2011, Chemale Jr. et al., 2011).

FIGURE 16

6.4.2 Post-collisional strain partitioning

Strain partitioning during progressive deformation is interpreted as responsible for tectonic juxtaposition of different crustal levels (Fig. 16c and d) and contrasting final structural picture characteristic of each domain (Fig. 16e). It is noteworthy that strike-slip structures prevail in the Major Gercino Shear Zone domain, while they are discrete along the entire Tijucas Fold Belt, which is considered a low-strain zone relative to the Major Gercino Shear Zone strike-slip tectonics (e.g. Florisbal et al., 2012c; Martini et al., 2015). Overall oblique transpression is partitioned into structural domains (Fig. 3 and 16), as illustrated in the deformation triangle (Fig. 16f) proposed by Jones et al. (2004).

At the Major Gercino Shear Zone, oblique transpression progressively evolved into strike-slip by rotation of foliation towards subvertical position due to asymmetric folds and progressive development of a transposition foliation. The transitional phase is marked by the structures decribed in the Quatro Ilhas Granitoids (625 – 615 Ma; Florisbal et al., 2012a), as gently-dipping and subvertical foliation, both bearing strike-parallel magmatic and stretching lineations (Fig. 16c). The Porto Belo Complex and Quatro Ilhas Granitoids are therefore considered to be part of the inner oblique-slip subdomain of MGSZ (as in Fig. 16e). Strike-slip is recorded in magmatic and high-T solid-state fabrics of sucessive intrusions younger than 615 Ma (Fig. 16d).

In the Tijucas Fold Belt, strain partitioning has led to decoupling of infrastructure and suprastructure. Exhumation of the Camboriú Complex migmatite was driven by partitioning of the contractional component of overall transpression and buoyancy of the magma-rich system around 635 Ma. At the same time, the southern Brusque Complex exhibits: i) locally high thermal gradient recorded by amphibolite-facies metamorphism along the Brusque– Camboriú interface, in contrast with the regional greenschist-facies conditions of the complex; ii) discrete antithetic extensional structures that result from reworking of the thrust-related main foliation (Fig. 10b and d); iii) domains locally overprinted by static metamorphism (Fig. 10e); and iv) a local strain gradient increasing towards the contact with the Camboriú Complex mylonites, where both complexes exhibit concordant, dextral plus normal, top-to-WSW, transtensional deformation (Fig. 11). All these features can be explained by the exhumation of the magma-rich, migmatitic Camboriú Complex (Fig. 16c) responsible for raising up the geothermal gradient.

The timing of this event for the Brusque Complex is indirectly constrained. The NW-verging, thrust-related fabric of this complex must have originated at ca. 650 – 645 Ma, coeval with the Porto Belo Complex main thrusting episode. The local extensional component is interpreted to have affected the Brusque Complex concomitantly with the Camboriú Complex exhumation, which should be bracketed by the crystallization of migmatite neosomes and Itapema Granite, and by the Rio Pequeno Granite emplacement, i.e. between ca. 635 – 625 Ma. Tectonic inversion is inferred to have occurred at ca. 635 Ma in the suprastructure. The extensional ductile structures of the southern Brusque Complex are considered to represent the ductile thinning of the suprastructure (e.g. Vanderhaeghe et al., 1999), related to the Camboriú Complex doming in the post-collisional period (Fig. 16c).

The exhumation/extrusion of the infrastructure is thought to have taken place while extension affected the suprastructure due to deformation partitioning during transpression, culminating in the juxtaposition of the Camboriú and Brusque complexes (Fig. 16a-c), as it is observed now (Fig. 16e). It is likely that the extrusion component of the transpressive deformation (in the sense of Fernández and Diaz-Azpiroz, 2009) was concentrated in the Camboriú Complex migmatites after strain partitioning, as a pure-shear domain (Fig. 16d).

A similar situation of migmatitic core extrusion due to transpression and strain partitioning is reported by Goscombe et al. (2005) for the Kaoko Belt, considered to be the counterpart of the northern Dom Feliciano

Belt in Africa (Konopásek et al., 2016), at 575 – 550 Ma. The high-grade Orogen Core unit of that belt is bound by a hanging wall transtensional shear zone and a footwall transpressive shear zone which separate it from the hinterland and from the foreland supracrustals, respectively. The result is an extrusion and juxtaposition of the Orogen Core unit with the shallower domains. The main difference is that, in our scenario, a slice of supracrustal rocks was trapped between the foreland infrastructure and the hinterland (Fig. 2 and 3), and thus records the heating PT-path (Fig. 15) caused by basement extrusion/exhumation.

The detachment of middle and upper crust in the studied case is recorded as a narrow shear zone. Within this zone, L-tectonites are locally developped over leucogranites of the Camboriú Complex along its southern boundary, whereas amphibolites of the Brusque Complex are concordantly deformed (Fig. 11). Constrictional fabric is common in rocks exhumed during oblique transtension (e.g. Krabbendam and Dewey, 1998), especially focused in materials moderately stronger than the surrounding rocks (Yang et al., 2019). In our case, it represents a local feature due to strain partitioning in the regional transpressive scenario, possibly due to the rheological interface established as the extruding migmatitic core cooled against the unroofing suprastructure. The detachment shows transtensional, dextral plus normal components as a consequence of relative movements of the structural domains, resulting in top-to-WSW general vergence (Fig. 11f to h).

The Rio Pequeno Granite (ca. 625 Ma) crosscuts the above-mentioned structure (Fig. 2 and 3) at low-strain conditions, while most of the deformation was focused in the Major Gercino Shear Zone. Later intrusions (after 615 Ma) are attributed to partial melting of sources similar to Camboriú Complex and associated supracrustal rocks (Florisbal et al., 2012b,c; Martini et al., 2015; Hueck et al., 2020). Fault-related rocks along the contact between Camboriú and Brusque complexes suggest that the whole system reached the brittle-ductile transition during exhumation (Fig. 11i and j).

6.5 Tectonic implications for the Dom Feliciano Belt evolution

Understanding the nature of the Major Gercino Shear Zone is key subject in the debate regarding the evolution of the Dom Feliciano Belt. The present model challenges some hypotheses from the literature concerning the interpretation of this shear zone as a suture, and the allochtonous or exotic character of the Florianópolis Batholith relative to the Tijucas Fold Belt (Basei et al., 2005; 2008; Hueck et al., 2018). This may be exemplified by the evidence of similar metamorphic and partial melting conditions of both Camboriú and Porto Belo complexes at upper amphibolite facies conditions (roughly 4 – 5 kbar and 700 – 750°C). It means that at ca. 650 – 635 Ma (Fig. 16a and b) these complexes were already juxtaposed. This time-span has been considered as an “early convergence” period which preceeded a supposed oblique collision at 615 – 585 Ma (e.g. Hueck et al., 2018). Ours, as well as other previously published data do not support such late crustal thickening, since this period (after 615 Ma) corresponds to the age of post-collisional granites successively emplaced along the Major Gercino Shear Zone, and synchronous to its dextral strike-slip movement (Bitencourt and Nardi, 1993; Chemale Jr. et al., 2012; Florisbal et al., 2012a; Peruchi, 2016).

The significance of the Major Gercino Shear Zone at pre-collisional times is still a matter of debate (see De Toni et al., 2020). The available data do not permit to rule out the presence of a suture zone older than 645 Ma, but no direct evidence of oceanic crust consumption (i.e. ophiolitic association) has been reported from the northern Dom Feliciano Belt so far. Based mostly on regional aerogeophysical data, Bruno et al. (2018) consider that the Itajaí-Perimbó Shear Zone, to the north (Fig. 1), rather than the Major Gercino Shear Zone, would be the boundary between unrelated basement domains. The Major Gercino Shear Zone is conceived by these authors as an intracontinental shear zone, in agreement with the previous hypothesis of Florisbal et al. (2012c).

7. Conclusions

Evaluation of geology, structures, available PT conditions and ages are integrated along a geological cross-section in the northern Dom Feliciano Belt, crossing from the hinterland Florianópolis Batolith towards the foreland Tijucas Fold Belt. The results are summarized as follows:

i) The structural pattern of the whole area follows a NE-to-ENE trend, with the early fabric preserved as S_1 foliation dipping gently towards SE or refolded into open to tight folds. This pattern is recognized in all structural domains, and together with variably plunging lineation is interpreted to record a NNW-verging oblique collision which affected the area at, or before, ca. 650 – 635 Ma.

ii) The oblique collision is recorded as a transpressional progressive deformation which led to strain partitioning into three structural domains: the Major Gercino Shear Zone, and the Tijucas Fold Belt suprastructural and infrastructural domains. These domains have absorbed different kinematic components, in agreement with theoretical and analogue models. Both lateral co-existence and temporal progression of tectonic regimes, usually from subhorizontal to subvertical foliations, and from highly oblique to strike-parallel lineations, are characteristic of triclinic transpressional deformation, as recorded in the geology of the studied cross-section.

iii) A progression from oblique transpression with inclined extrusion (Porto Belo Complex, 650 – 645 Ma, at ca. 707 °C/3.7 – 4.8 kbar), through a tangential regime (Quatro Ilhas Granitoids, 625 – 615 Ma) towards strike-slip tectonics (Mariscal Granite and younger intrusions, after ca. 615 Ma), is recorded along the Major Gercino Shear Zone.

iv) The Camboriú Complex is considered to be part of a pure shear-dominated domain, where the contractional component is documented by alternating shear sense of asymmetric objects, absence of lineation, upright, double-plunging, symmetric folding and conjugate, axial planar shear cleavage. The complex records regional doming and exhumation from at least 5 kbar (possibly deeper than 6 kbar) up to 3.4 kbar, assisted by the buoyancy of high proportions of melt (at 635 Ma or shortly after), and interpreted to result from the oblique extrusion component of the system.

v) Slightly delayed age values point to a possible diachronic evolution with partial melting and oblique collisional deformation starting some million years earlier in the hinterland (Major Gercino Shear Zone) and propagating towards the foreland infrastructure.

vi) At the same time, pervasive greenschist-facies, NW-directed thrusting of the southern Brusque Complex is followed by a discrete amphibolite-facies fabric, which developed around 635 Ma, during the Camboriú Complex upwelling. The thermal effect of its exhumation over the Brusque Complex is documented as localized transposition zones close to the contact with the migmatites, and along static, contact metamorphic domains. Both higher geothermal gradient and local tectonic inversion are interpreted as results of the Camboriú Complex doming/extrusion related to transpressional strain partitioning.

The Major Gercino Shear Zone is conceived as an intracontinental shear zone which has focused syntectonic emplacement of post-collisional magmas and absorbed the dextral strike-slip component of the overall oblique transpression. This major tectonic event has affected infra- and suprastructure of theTijucas Fold Belt, as well as the Florianópolis Batholith and its basement, both considered to have been contiguous blocks at least since 650 – 645 Ma.

8. Acknowledgements

The authors acknowledge financial support of the Brazilian National Research Council (CNPq) through the productivity grants to M.F. Bitencourt (311486/2015-0) and L.V.S. Nardi (306605/2018-0), and through the Universal Project N° 481841/2012-1 (M.F. Bitencourt). PhD scholarship to G.B. De Toni (141011/2015-7) was also financed by CNPq. The authors acknowledge Coordenação de Aperfeiçoamento de Pessoal Docente for funding of the CAPES (Brazil) – SIU (Norway) cooperation program (CAPES - 88881.117872/2016-01 and 88887.141226/2017-00, SIU – TF-2016-CAPES-SIU/10024). J Konopásek appreciates financial support of the Czech Science Foundation (grant no. 18-24281S). We thank Kai Neufeld and Susan Drago for their kind help with EDSB at UiT and microprobe analyses at UFRGS, respectively. The authors are also grateful to an anonymous reviewer and C. Fernández, whose critical reviews and comments have lead to significant improvement of this work.

References

Andersen, T.B., 1998. Extensional tectonics in the Caledonides of southern Norway, an overview. Tectonophysics, 285, 333-351.

Arena, K.R., Hartmann, L.A., Lana, C., 2016. Evolution of neoproterozoic ophiolites from the southern Brasiliano Orogen revealed by zircon U-Pb-Hf isotopes and geochemistry. Precambrian Research, 285, 299–314.

Asvald, C. 2018. Metamorphic evolution in external zones of the Dom Feliciano-Kaoko orogenic system. Unpublished Master Thesis. The Arctic University of Norway. 82p. Avaliable at: https://munin.uit.no/handle/10037/12816

Basei, M.A.S., Frimmel, H.E., Nutman, A.P., Preciozzi, F., Jacob, J., 2005. The connection between the Neoproterozoic Dom Feliciano (Brazil/Uruguay) and Gariep (Namibia/South Africa) orogenic belts. Precambrian Research, 139, 139–221.

Basei, M.A.S., Frimmel, H.E., Nutman, A.P., Preciozzi, F., 2008. West Gondwana amalgamation based on detrital zircon ages from Neoproterozoic Ribeira and Dom Feliciano belts of South America and comparison with coeval sequences from SW Africa. In: Pankhurst, R.J., Trouw, R.A.J., de Brito Neves, B.B., de Wit, M.J. (eds) West Gondwana: Pre-Cenozoic Correlations Across the South Atlantic Region, London. Geological Society London, Special Publication 294, pp 239–256.

Basei, M.A.S., Campos Neto, M.C., Castro, N.A., Nutman, A.P., Wemmer, K., Yamamoto, M.T., Hueck, M., Osako, L., Siga, O., Passarelli, C.R., 2011. Tectonic evolution of the Brusque group, Dom Feliciano belt, Santa Catarina, Southern Brazil. Journal of South American Earth Sciences, 32(4), 324–350.

Basei, M.A.S., Campos Neto, M.C., Lopes, A.P., Nutman, A.P., Liu, D., Sato, K., 2013. Polycyclic evolution of Camboriú Complex migmatites, Santa Catarina, Southern Brazil: integrated Hf isotopic and U-Pb age zircon evidence of episodic reworking of a Mesoarchean juvenile crust. Brazilian Journal Geology, 43, 427–443.

Battisti, M.A., Bitencourt, M.F., De Toni, G.B., Nardi, L.V.S, Konopásek, J., 2018. Metavolcanic rocks and orthogneisses from Porongos and Várzea do Capivarita complexes: A case for identification of tectonic interleaving at different crustal levels from structural and geochemical data in southernmost Brazil. Journal of South American Earth Sciences, 88, 253-274.

Bettucci, L.S., Burgueño, A.M., 1993. Análisis sedimentológico y faciológico de la Formación Rocha (ex Grupo Rocha). Revista Brasileira de Geociências, 23, 323-329.

Bitencourt, M.F., 1996. Granitóides sintectônicos da região de Porto Belo, SC: uma aboradagem petrológica e estrutural do magmatismo em zonas de cisalhamento. Tese de Doutorado, Instituto de Geociências, Universidade Federal do Rio Grande do Sul, 310 pp.

Bitencourt, M.F., Nardi, L.V.S. 1993. Late- to Post-collisional Brasiliano Magmatism in Southernmost Brazil. Anais da Academia Brasileira de Ciências, 65, 3-16.

Bitencourt, M.F., Nardi, L.V.S., 2000. Tectonic setting and sources of magmatism related to the Southern Brazilian Shear Belt. Revista Brasileira de Geociências 30, 186–189.

Bitencourt, M.F., Nardi, L.V.S., 2004. The role of xenoliths and flow segregation in the genesis and evolution of the Paleoproterozoic Itapema Granite: a crustally-derived magma of shoshonitic affinity from Southern Brazil. Lithos 73, 01–19.

Blundy, J. D. & Holland, T.J.B. 1990. Calcic amphibole equilibria and a new amphibole plagioclase geothermometer. Contributions to Mineralogy and Petrology, 104, 208-224.

Bruno, H., Almeida, J., Heilbron, M., Salomão, M., Cury, L., 2018. Architecture of major precambrian tectonic boundaries in the northern part of the Dom Feliciano Orogen, southern Brazil: Implications for the West Gondwana amalgamation. Journal of South American Earth Sciences, 86, 301-317.

Burchfiel, B.C., Z. Chen, Hodges, K.V., Y. Liu, Royden, L.H., C. Deng, J. Xu, 1992. The South Tibetan Detatchment System, Himalayan Orogen: Extension Contemporaneous with and Parallel to Shortening in a Collisional Mountain Belt. Geological Society of America Special Paper, 269.

de Campos RS, Philipp RP, Massonne HJ, Chemale F Jr, Theye T, 2012. Petrology and isotope geology of mafic to ultramafic metavolcanic rocks of the Brusque Metamorphic Complex, southern Brazil. International Geology Reviews, 54(6), 686–713

Chemale Jr., F., Philipp, R.P., Dussin, I.A., Formoso, M.L.L., Kawashita, K., Berttotti, A.L., 2011. Lu-Hf and U-Pb age determination of Capivarita anorthosite in the Dom Feliciano Belt, Brazil. Precambrian Research. 186, 117-126

Chemale Jr., F., Mallmann, G., Bitencourt, M.F., Kawashita, K., 2012. Time constraints on magmatism along the Major Gercino Shear Zone, southern Brazil: implications for West Gondwana reconstruction. Gondwana Research 22 (1), 184–199.

Connolly, J.A.D., 2005. Computation of phase equilibria by linear programming: a tool for geodynamic modeling and its application to subduction zone decarbonation. Earth and Planetary Science Letters, 236(1–2), 524–541

Czeck, D.M., Hudleston, P.J., 2003. Testing models for obliquely plunging lineations in transpression: a natural example and theoretical discussion. Journal of Structural Geology 25, 959-982.

Dewey, J.F., Holdsworth, R.E., Strachan, R.A., 1998. Transpression and transtension zones. In: Holdsworth, R.E., Strachan, R.A., Dewey, J.F. (Eds.), Continental Transpressional and Transtensional Tectonics. Special Publication of the Geological Society, London 135, pp. 1–14.

De Toni, 2019. Correlação geológico-estrutural e modelo integrado de evolução para o Cinturão Dom Feliciano sob transpressão inclinada no Neoproterozoico do sul do Brasil. Unpublished PhD thesis. Universidade Federal do Rio Grande do Sul.

De Toni, G.B., Bitencourt, M.F., Nardi, L.V.S, Florisbal, L.M., Almeida, B.S., Geraldes, M., 2020. Dom Feliciano Belt orogenic cycle tracked by its pre-collisional magmatism: the Tonian (ca. 800 Ma) Porto Belo Complex and its correlations in southern Brazil and Uruguay . Precambrian Research, accepted for publication. https://doi.org/10.1016/j.precamres.2020.105702

Dragone, G N, Ussami, N, Gimenez, M E, Klinger, F G L, Chaves, C A M, 2017. Western Parana suture/shear zone and the limits of Rio Apa, Rio Tebicuary and Rio de la Plata cratons from gravity data. Precambrian Research, 291, 162–177.

Egydio-Silva, M., Vauchez, A., Raposo, M.I.B., Bascouc, J., Uhleind, A., 2005. Deformation regime variations in an arcuate transpressional orogeny (Ribeira belt, SE Brazil) imaged by anisotropy of magnetic susceptibility in granulites. Journal of Structural Geology, 27, 1750-1764.

Fernandes, L.A.D., Tommasi, A., Porcher, C.C., 1992. Deformation patterns in the southern Brazilian branch of the Dom Feliciano Belt: a reappraisal. Journal of South American Earth Sciences, 5, 77-96.

Fernandes, L.A.D., Menegat, R., Costa, A.F.U., Koester, E., Kramer, G., Tommasi, A., Porcher, C.C., Ramgrab, G.E., Camozzato, E., 1995a. Evolução tectônica do Cinturão Dom Feliciano no Escudo Sul-rio-grandense: Parte I – uma contribuição a partir do registro geológico. Revista Brasileira Geociências 25, 351-374.

Fernandes, L.A.D., Menegat, R., Costa, A.F.U., Koester, E., Kramer, G., Tommasi, A., Porcher, C.C., Ramgrab, G.E., Camozzato, E., 1995b. Evolução tectônica do Cinturão Dom Feliciano no Escudo Sul-rio-grandense: Parte II – uma contribuição a partir das assinaturas geofísicas. Revista Brasileira Geociências 25, 375-384.

Fernández, C., Díaz-Azpiroz, M., 2009. Triclinic transpression zones with inclined extrusion. Journal of Structural Geology 31, 1255-1269.

Fernández, C., Czeck, D.M., Díaz-Azpiroz, M., 2013. Testing the model of oblique transpression with oblique extrusion in two natural cases: Steps and consequences. Journal of Structural Geology, 54, 85-102.

Fischer, G., Fassbinder, E., Barros, C.E.M., Fossen, H., 2019. The evolution of quartz veins during the tectonometamorphic development of the Brusque Metamorphic Complex, Brazil. Journal of South American Earth Sciences 93, 174–182.

Florisbal, L.M., Bitencourt, M.F., Janasi, V.A., Nardi, L.V.S., Heaman, L.M., 2012a. Petrogenesis of syntectonic granites emplaced at the transition from thrusting to transcurrent tectonics in post-collisional setting: whole-rock and Sr–Nd–Pb isotope geochemistry in the Neoproterozoic Quatro Ilhas and Mariscal granites, southern Brazil. Lithos 153, 53–71.

Florisbal, L.M., Janasi, V.A., Bitencourt, M.F., Heaman, L.M., 2012b. Space–time relation of post-collisional granitic magmatism in Santa Catarina, southern Brazil: U–Pb LA-MC-ICP-MS zircon geochronology of coeval mafic-felsic magmatism related to the Major Gercino Shear Zone. Precambrian Research, 216, 132–151.

Florisbal, L.M., Janasi, V.A., Bitencourt, M.F., Nardi, L.V.S., Heaman, L.M., 2012c. Contrasted crustal sources as defined by whole-rock and Sr–Nd–Pb isotope geochemistry of Neoproterozoic early post-collisional granitic magmatism within the Southern Brazilian Shear Belt, Camboriú, Brazil. Journal of South American Earth Sciences, 39, 24–43.

Fossen, H., Rykkelid, E. 1992. Post-collisional extension of the Caledonide orogen in Scandinavia: structural expressions and tectonic significance. Geology, 20, 737-740.

Fossen, H., Tikoff, B., 1993. The deformation matrix for simultaneous simple shearing, pure shearing and volume change, and its application to transpression–transtension tectonics. Journal of Structural Geology, 15, 413–422.

Goodwin, L.B., Williams, P.F., 1996. Deformation path partitioning within a transpressive shear zone, Marble Cove, Newfoundland. Journal of Structural Geology 18, 975-990.Goscombe, B., Gray, D., Hand, M., 2005. Extrusional Tectonics in the Core of a Transpressional Orogen; the Kaoko Belt, Namibia. Journal of Petrology, 46(6), 1203-1241.

Gregory, T.R., M.F., Bitencourt, Nardi, L. V., Florisbal, L. M, Chemale, F. Jr. 2015. Geochronological data from TTG-type rock associations of the Arroio dos Ratos Complex and implications for crustal evolution of southernmost Brazil in Paleoproterozoic times. Journal of South American Earth Science. 57, 49–60.

Guadagnin, F., Chemale Jr., F., Dussin, I.A., Jelinek, A.R., Santos, M.N., Borba, M.L., Justino, D., Bertotti, A.L., Alessandretti, L., 2010. Depositional age and provenance of the Itajaí Basin, Santa Catarina State, Brazil: implications for SW Gondwana correlation. Precambrian Research, 180, 156–182.

Harland, W.B., 1971. Tectonic transpression in Caledonian Spitzbergen. Geological Magazine 108, 27–42.

Harris, L.B., Koyi, H.A., Fossen, H., 2002. Mechanisms for folding of high-grade rocks in extensional tectonic settings. Earth-Science Reviews, 59, 163-210.

Hartmann, L. A., Santos, J. O. S., Mcnaughton, N. J., Vasconcellos, M.A.Z., Silva, L.C., 2000. Ion microprobe (SHRIMP) dates complex granulite from Santa Catarina, southern Brazil. Anais da Academia Brasileira de Ciências, Rio de Janeiro, 72(4), 560-572,.

Hartmann, L.A., Bitencourt, M.F., Santos, J.O., McNaughton, N.J., Rivera, C.B., Betiollo, L., 2003. Prolonged Paleoproterozoic magmatic participation in the Neoproterozoic Dom Feliciano belt, Santa Catarina, Brazil, based on zircon U–Pb SHRIMP geochronology. Journal of South American Earth Science 16, 477–492.

Hasui, Y., Carneiro, C.D.R., Coimbra, A.W., 1975. The Ribeira folded belt. Revista Brasileira de Geociências, 5, 257–266.

Höfig, D.F., Marques, J.C., Basei, M.A.S., Giusti, R.O., Kohlrausch, C., Frantz, J.C., 2017. Detrital zircon geochronology (U-Pb LA-ICP-MS) of syn-orogenic basins in SW Gondwana: new insights into the cryogenian-ediacaran of Porongos complex, Dom Feliciano belt, southern Brazil. Precambrian Research, 306, 189-208.

Holdsworth, R.E., Tavarnelli, E., Clegg, P., Pinheiro, R.V.L., Jones, R.R., McCaffrey, K.J.W., 2002. Domainal deformation patterns and strain partitioning during transpression: an example from the Southern Uplands terrane, Scotland. Journal of the Geological Society of London 159, 401–415.

Holland, T.J.B., Blundy, J.D., 1994, Non-ideal interactions in calcic amphiboles and their bearing on amphibole-plagioclase thermometry: Contributions to Mineralogy and Petrology, v. 116, p. 433–447.

Holland, T.J.B., Powell, R., 1998. An internally consistent thermodynamic data set for phases of petrological interest. Journal of Metamorphic Geology, 16, 309–343.

Hueck, M., Basei, M.A.S., de Castro, N.A., 2016. Origin and evolution of the granitic intrusions in the Brusque Group of the Dom Feliciano Belt, south Brazil: Petrostructural analysis and whole-rock/isotope geochemistry. Journal of South American Earth Sciences, 69, 131–151.

Hueck, M., Basei, M.A.S., Wemmer, K., Oriolo, S., Heidelbach, F., Siegesmund, S., 2018. Evolution of the Major Gercino Shear Zone in the Dom Feliciano Belt, South Brazil, and implications for the assembly of southwestern Gondwana. International Journal of Earth Sciences, 108(2), 403-425.

Hueck, M., Base, M.A.S., Castro, N.,A., 2020. Tracking the sources and the evolution of the late Neoproterozoic granitic intrusions in the Brusque Group, Dom Feliciano Belt, South Brazil: LA-ICP-MS and SHRIMP geochronology coupled to Hf isotopic analysis. Precambrian Research, 338, 105566.

Jones, R.R., Holdsworth, R.E., Clegg, P., McCaffrey, K., Tavarnelli, E., 2004. Inclined transpression. Journal of Structural Geology 26, 1531–1548.

Jost, H., Bitencourt, M.F., 1980. Estratigrafia e tectônica de uma fração da Faixa de Dobramentos Tijucas no Rio Grande do Sul. Acta Geológica Leopoldensia, 4(7), 27-60.

Jost, H., Hartmann, L.A., 1984. Província Mantiqueira – Setor Meridional. in: Almeida, F.F.M., Hasui, Y. (Eds.), Pré-Cambriano do Brasil. Editora Edgard Blucher, São Paulo. p. 345-368.

Koester, E, Porcher, C.C., Pimentel, M.M., Fernandes, L.A.D., Vignol-Lelarge, M.L., Oliveira, L.D., Ramos, R.C., 2016. Further evidence of 777 Ma subduction-related continental arc magmatism in Eastern Dom Feliciano Belt, southern Brazil: The Chácara das Pedras Orthogneiss. Journal of South American Earth Sciences, 68, 155-166.

Konopásek, J., Sláma, J., Košler, J., 2016. Linking the basement geology along the Africa–South America coasts in the South Atlantic. Precambr Res 280, 221–230.

Konopásek, J., Janoušek, V., Oyhantçabal, P., Sláma J ., Ulrich, S., 2018. Did the circum-Rodinia subduction trigger the Neoproterozoic rifting along the Congo–Kalahari Craton margin? International Journal of Earth Sciences 107, 1859–1894. https://doi.org/10.1007/s00531-017-1576-4

Krabbendam, M., Dewey, J.F., 1998. Exhumation of UHP rocks by transtension in the Western Gneiss Region, Scandinavian Caledonides. Geological Society, London, Special Publications, 135:159-181

Leite, J.A.D., Hartman, L.A., Mcnaughton, N.J., Chemale Jr., F., 1998. SHRIMP U/Pb Zircon Geochronology of Neoproterozoic Juvenile and Crustal-Reworked Terranes in Southernmost Brazil, International Geology Review, 40(8), 688-705.

Lenz C., Fernandes, L.A.D., McNaughton, N.J., Porcher, C.C., Masquelin, H., 2011. U–Pb SHRIMP ages for the Cerro Bori orthogneisses, Dom Feliciano Belt in Uruguay: evidences of a ~ 800 Ma magmatic and ~ 650 Ma metamorphic event. Precambrian Research 185, 149–163.

Liégeois, J.P., 1998. Some words on the post-collisional magmatism. Preface to Special Edition on Post-Collisional Magmatism. Lithos 45, xv–xvii.

Martil, M.M.D., 2016. O magmatismo de arco continental pré-colisional (790 ma) e a reconstituição espaço-temporal do regime transpressivo (650 Ma) no Complexo Várzea do Capivarita, sul da Província

Mantiqueira. PhD thesis. Universidade Federal do Rio Grande do Sul. Avaliable at: https://lume.ufrgs.br/handle/10183/149194

Martil, M.M.D., Bitencourt, M.F., Nardi, L.V.S., Koester, E., Pimentel, M.M., 2017. Pre-collisional, Neoproterozoic (ca. 790 Ma) continental arc magmatism in southern Mantiqueira Province, Brazil: geochemical and isotopic constraints from the Várzea do Capivarita Complex. Lithos 274–275, 39–52.

Martini, 2019. Migmatitos e a geração de granitos no Complexo Camboriú, SC: controle estrutural, condições de fusão da crosta e gênese do Granito Itapema. PhD thesis. Universidade Federal do Rio Grande do Sul. Porto Alegre, Brazil. 210 pp. Avaliable at: https://lume.ufrgs.br/handle/10183/189058

Martini, A., Bitencourt, M.F., Nardi, L.V.S., Florisbal, L.M., 2015. An integrated approach to the late stages of Neoproterozoic post-collisional magmatism from Southern Brazil: Structural geology, geochemistry and geochronology of the Corre-mar Granite. Precambrian Research, 261, 25-39.

Martini, A., Bitencourt, M.F., Weinberg, R., De Toni, G.B. Nardi, L.V.S., 2019a. From migmatite to magmas - crustal melting and generation of granite in the Camboriu Complex, south Brazil. Lithos, 340–341:270–286.

Martini, A., Bitencourt, M.F., Weinberg, R., De Toni, G.B, 2019b. Melt-collecting structures and the formation of extraction dykes during syntectonic anatexis of the Camboriú Complex, south Brazil. Journal of Structural Geology, 127:103866.

Molina, J.F., Moreno, J.A., Castro, A., Rodríguez, C., Fershtater, G.B., 2015. Calcic amphibole thermobarometry in metamorphic and igneous rocks: New calibrations based on plagioclase/amphibole Al-Si partitioning and amphibole/liquid Mg partitioning. Lithos, 232, 286-305.

Oriolo, S., Oyhantçabal, P., Wemmer, K., Heidelbach, F., Pfänder, J., Basei, M.,A.,S., Hueck, M., Hannich, F., Sperner, B., Siegesmund, S., 2016. Shear zone evolution and timing of deformation in the Neoproterozoic transpressional Dom Feliciano Belt, Uruguay. Journal of Structural Geology, 92, 59–78.

Oriolo, S, Oyhantçabal, P, Wemmer, K, Siegesmund, S, 2017. Contemporaneous assembly of Western Gondwana and final Rodinia break-up: implications for the supercontinent cycle. Geoscience Frontiers, 8, 1431–1445.

Oyhantçabal, P., Siegesmund, S., Wemmer, K., Presnyakov, S., Layer, P., 2009. Geochronological constraints on the evolution of the southern Dom Feliciano Belt (Uruguay). Journal of the Geological Society of London, 166, 1075–1084.

Paim, P.S.G., Chemale Jr., F., Wildner, W., 2014. Estágios evolutivos da Bacia do Camaquã (RS). Ciência e Natura, Santa Maria, v. 36 p. 183–193.

Peruchi, F.M., 2016. Evolução espaço-tempo do Granodiorito Estaleiro, região de Porto Belo, SC. Unpublished graduation thesis. Universidade Federal de Santa Catarina, Brazil. 81 pp. Avaliable at: https://repositorio.ufsc.br/handle/123456789/173323

Peternell, M., Bitencourt, M.F., Kruhl, J.H., Stab, C., 2010. Macro- and microstructures as indicators of developmentof syntectonic granitoids and host rocks in the Camboriú region, Santa Catarina, Brazil. Journal of South American Earth Sciences 29:738-750.

Philipp, R.P., Mallmann, G., Bitencourt, M.F., Souza, E.R., Liz, J.D., Wild, F., Arend, S., Oliveira, A.S., Duarte, L.C., Rivera, C.B., Prado, M., 2004. Caracterização Litológica e Evolução Metamórfica da Porção Leste do Complexo Metamórfico Brusque, Santa Catarina: Revista Brasileira de Geociências, v. 34(1), 21–34.

Philipp, R.P., de Campos, R.S., 2010, Granitos peraluminosos intrusivos no Complexo Metamórfico Brusque: Registro do magmatismo relacionado a colisão Neoproterozóica no Terreno Tijucas, Itapema, SC: Revista Brasileira de Geociências, 40(3), 301–318.

Philipp, R.P., Pimentel, M.M., Chemale Jr., F., 2016. Tectonic evolution of the Dom Feliciano Belt in Southern Brazil: Geological relationships and U-Pb geochronology. Brazilian Journal of Geology, 46(1), 83–104

Philipp, R.P., Pimentel, M.M., Basei, M.A.S., 2018. The Tectonic Evolution of the São Gabriel Terrane, Dom Feliciano Belt, Southern Brazil: The Closure of the Charrua Ocean. In: S. Siegesmund, S., Basei, M.A.S., Oyhantçabal, P., Oriolo, S. (eds.). Geology of southwest gondwana, Regional geology reviews, Springer, Heidelberg, pp 243–265

Philippon, M., Corti, G., 2016. Obliquity along plate boundaries. Tectonophysics, 693, 171-182.

Ramos, R.C., Koester, E., Triboli, D.V., Porcher, C.C., Gezatt, J.N., Silveira, R.L., 2018. Insights on the evolution of the Arroio Grande Ophiolite (Dom Feliciano Belt, Brazil) from Rb-Sr and SHRIMP U-Pb isotopic geochemistry. Journal of South American Earth Sciences, 86, 38-53.

Rivera, C.B., Bitencourt, M.F., Nardi, L.V.S., 2004. Integração de parâmetros físicos do magma e composição química dos minerais na petrogênese do Granito Itapema, SC. Revista Brasileira de Geociências, 34, 361-372.

Robin, P.-Y.F., Cruden, A.R., 1994. Strain and vorticity patterns in ideally ductile transpression zones. Journal of Structural Geology 16, 447–466.

Saalmann, K., Remus, M.V.D., Hartmann, L.A., 2006. Structural evolution and tectonic setting of the Porongos Belt, southern Brazil. Geological Magazine, 143(1), 59-88.

Saalmann K, Gerdes A, Lahaye Y, Hartmann LA, Remus MVD, Läufer A, 2011. Multiple accretion at the eastern margin of the Rio de la Plata craton: the prolonged Brasiliano orogeny in southernmost Brazil. International Journal of Earth Sciences, 100, 355–378.

Sanderson, D.J., Marchini, W.R.D., 1984. Transpression. Journal of Structural Geology 6, 449–458.

Sawyer, E.W., 2008. Atlas of migmatites. Canadian Mineralogist, Special Publication 9. Mineralogical Association of Canada, 386 pp.

Schmidt, M. W. 1992. Amphibole composition in tonalite as a function of pressure: an experimental calibration of the Al-in-hornblende barometer. Contributions to Mineralogy and Petrology, 110, 304-10.

Silva, L.C., 1991. O cinturão metavulcanossedimentar Brusque e a evolução policíclica das faixas dobradas proterozóicas no sul do Brasil: uma revisão. Revista Brasileira de Geociências, 21, 60–73.

Tikoff, B., Teyssier, C., 1994. Strain modeling of displacement field partitioning in transpressional orogens. Journal of Structural Geology, 11, 1575-1588.

UFRGS, 2000. Mapeamento Geológico 1:25 000: Projeto Camboriú, 6 vol. Trabalho de Graduação do Curso de Geologia, Instituto de Geociências, Universidade Federal do Rio Grande do Sul.

Vanderhaeghe, O., Burg, J.-R., Teyssier, C. 1999. Exhumation of migmatites in two collapsed orogens: Canadian Cordillera and French Variscides. In: Ring, U., Brandon, M. T., Lister, G. S. & Wilett, S. D. (eds)

Exhumation Processes: Normal Faulting, Ductile Flow and Erosion. Geological Society, London, Special Publications, 154, 181-204.

Weinberg, R.F., Hasalová, P., Ward, L., Fanning, C.M., 2013. Interaction between deformation and magma extraction in migmatites: Examples from Kangaroo Island, South Australia. Geological Society of America Bulletin, 125(7-8), 1282-1300.

Weinberg, R.F., Hasalová, P., 2015. Water-fluxed melting of the continental crust: A review. Lithos 212-215, 158-188.

Will, T.M., Gaucher, C., Ling, X.-H., Li, X.-H., Li, Q.-L., Frimmel, H.E. 2019. Neoproterozoic magmatic and metamorphic events in the Cuchilla Dionisio Terrane, Uruguay, and possible correlations across the South Atlantic. Precambrian Research, 320, 303-322.

Yang, R., Jiang, D., Lu, L.X., 2019. Constrictional strain and linear fabrics as a result of deformation partitioning: a multiscale modeling investigation and tectonic significance. Tectonics, 38(8), 2829-2949.

Zibra, I., Smithies, R.H., Wingate, M.T.D, Kirkland, C.L., 2014. Incremental pluton emplacement during inclined transpression. Tectonophysics, 623, 100-122.

FIGURE CAPTIONS

Fig. 1 – (a) Geotectonic sketch of Western Gondwana (modified from Oriolo et al., 2017; Dragone et al., 2017; Will et al., 2019). (b)Geotectonic sketch of southern Brazil and Uruguay showing the Dom Feliciano Belt and cratonic adjacent areas (modified from Bitencourt and Nardi, 2000, Ramos et al., 2018; Will et al., 2019). (c) Santa Catarina shield area geological map (modified from Bitencourt and Nardi, 2004) with location of studied area shown in figure 2.

Fig. 2 – Porto Belo – Camboriú geological map (modified from Florisbal et al., 2012a, after Bitencourt, 1996; UFRGS, 2000; Philipp et al., 2004). The location of individual sections described in the paper and integrated in the composite section of figure 3 is shown.

Fig. 3 – Porto Belo – Camboriú composite cross-section. Notice that 340°- 160° is the cross-section orientation for Major Gercino Shear Zone and Brusque Complex structural domains, while it is changed for 320° - 140° in the Camboriú Complex. Location of the individual sections is presented, as well as stereonets representative of the main subdomains presented in the text.

Fig. 4 – Quatro Ilhas Granitoids general features at Ponta de Fora outcrop. (a) Quatro Ilhas Granitoids typical aspect at NW-SE subvertical section approximately perpendicular to the lineation and to fold axis (fold profile). The asymmetry of the fold indicate top-to-the-NW. (b) Detail of figure 4a, where it is possible to observe the heterogeneity of deformation along originally textural/compositional distinct layers. Central layer present a stronger foliation and K-feldspar porphyroclasts with well-developed recrystallization tails indicating top-to-the-NW sense of shear. (c) Stereonet presenting contoured pole-to-foliation of Quatro Ilhas Granitoids and linear fabrics: mineral (L_{Kf}) and stretching lineation (L_x) plus fold axis (B). (d) Horizontal section, approximately XZ-parallel, showing highly asymmetric structures such as S-C-C' (see sketch) and dextral, asymmetrical porphyroclasts, which recrystallization tails define a discontinuous banding along the

S-C mylonitic foliation. C' are discrete planes mostly developed in the central portion of the picture (see sketch).

Fig. 5 – Porto Belo Complex general features at Ponta das Bombas area. (a) Ponta das Bombas main outcrop, 340° - 160° cross-section, presenting the lithology distribution and main structural features. Samples sites and references to pictures are indicated. (b) Overview of the central portion of the same outcrop. The main antiformal structure of the outcrop is expressed by its morphology, with both limbs and the axial plane dipping towards SSE. In the far-right portion of the picture the bigger tabular gneissic body (Fig. 5c) can be observed. (c) Orthogneiss (melanosome) tabular body along the main foliation of the leucocratic granite. The granite intrudes the orthogneiss as cm-size veins which are folded and boudinaged, probably due to high-obliquity original contacs. Fold axis is indicated. (d) Typical aspect of a metatexitic migmatite along an oblique exposition, with interleaving of igneous and metamorphic rocks along the main banding, crossed by a leucogranitic vein. The vein presents very irregular and diffuse contacts with the migmatite, interfingering with some bands with textural continuity (inset). A simplified sketch is presented in the lower-left portion of the figure. (e) Typical aspect of a diatexitic migmatite in an approximately horizontal exposition. The dog for scale is 75 cm long. Outcrop located *ca.* 100 m south of the portion represented in figure 5a.

Figure 6 – Petrographic aspects and microstructures from Porto Belo Complex rocks. (a) Foliated leucogranite with biotite schlieren (sample GB-01A). Notice the presence of fine-grained, quartz-feldsphatic, recrystallized matrix. Dextral porphyroclasts are observed in the central portion. The section is subhorizontal, XZ plane. (b) Detail of the schlieren from figure 6a. Notice the hinge zone marked by a coarse-grained, kinked biotite grain, in the center of the picture. Very fine-grained mica occur due to low-temperature recrystallization. (c) Banded biotite monzogranite (metatexite – GB-01C) general view, with recrystalizated matrix between igneous relicts (upper portion). Asymmetric porphyroclasts indicate dextral shear sense. The lower porphyroclast show an incomplete boudinage (see inset). The section is

subhorizontal, XZ plane. (d) Foliated biotite hornblende tonalite with epidote (GB-01E). Notice the pair of subhedral hornblende and plagioclase crystals at the center, the first partially replaced by biotite. Recrystallized quartz grains present polygonal granoblastic texture. (e) General view of the tonalitic biotite orthogneiss (GB-01B), presenting a fine-grained granoblastic fabric and the contrastant texture of a titanite-bearing pocket leucosome, which asymmetry points the top-to-the-NW sense of shear. The section is subvertical, XZ plane. (f) Aspect of a tonalitic biotite orthogneiss (sample PB-57G, from Mariscal Beach) from a dextral, strike-slip high-strain zone, with fine-grained, quartz-feldspathic, granoblastic matrix.

Fig 7 – Structures from Porto Belo Complex at Ponta das Bombas area. (a) Diatexite with calc-silicate fragments and other enclaves showing top-to-NNW apparent movement. Same area of figure 5e. (b) Migmatitic orthogneiss heterogeneous deformation. Small patches with titanite-bearing leucogranitic material are interpreted as in situ pocket melts (see inset). The central, darker area presents diffuse and elongated patches, indicative of higher strain. The lower portion presents the surrounding leucogranite with schlieren. (c) Stereonet from Porto Belo Complex at Ponta das Bombas, presenting contoured pole to foliation, mineral/stretching lineations (L_{min}/L_x), poles to axial planes and fold axis (B). Equal area, lower hemisphere projection. (d) Vertical section, fold profile showing asymmetric, isoclinal folded metatexite with an orthogneissic melanosome presenting a sigmoid shape indicative of top-to-NNW thrust component. Location is *ca.* 50 m south of the portion represented in figure 5a. (e) Convolutely folded metatexite presenting subvertical axial planes truncated by discrete subhorizontal structures. (f) Disarmonic fold developed in metatexite. The central portion presents the coincidence of an antiform and a sinform hinge zone, culminating with a dilatant site filled with milky quartz. The upper portion of the picture (inset) shows top-to-NNW shear sense marked by transposition shear zones, with a duplex structure at outcrop scale.

Fig. 8 –Porto Belo Complex and Quatro Ilhas Granitoids contact relationships. (a) General overview with Porto Belo Complex migmatites at lower-right half of the picture, and Quatro Ilhas Granitoids at upper-left.

Notice the metatexite at first plan (lower portion of the picture), grading to the granitic injection which crosscuts the contact between the units and the Quatro Ilhas Granitoids foliation in the upper portion of the outcrop. (b) Detail of the intrusive contact of the leucogranitic injection crosscutting both the contact and the igneous foliation of the Quatro Ilhas Granitoids. Note that to the left of the injection there is a fragment of migmatite surrounded by the porphyritic Quatro Ilhas Granite. (c) Horizontal view of the lower portion from figure 08a, with the gradual to diffuse contact between the metatexite and the leucogranitic injection rooted in its main banding. (d) Vertical view, detail from figure 8b, with the porphyritic Quatro Ilhas Granite partially assimilating and disrupting the Porto Belo Complex metatexite. Notice the Quatro Ilhas Granite cm-size porphyroclasts.

Figure 9 – General aspects of volcano-sedimentary rocks of southern Brusque Complex along E – E' section. (a) E – E' cross-section with the recognized rock types and major structural elements. (b) Cross-section (160° - 340°) at Grossa Beach with the main structural features and localization of samples, detailed sketches and pictures. (c) Stereonet for contoured pole to foliation (S_x), pole to axial planes, stretching/mineral lineations (Lx/Lmin – see text for descriptions) and fold axis (B). Equal area, lower hemisphere projection. (d) Sketch from the central portion of the outcrop from figure 9b, presenting asymmetric to recumbent folds developed over calc-silicate and schist layers, as well as slightly oblique cm-wide leucogranitic earlier injections. Later leucogranitic injections crosscuts the folded layers. Intrafolial folds are locally preserved along schistosity and represent a pre-S_x structure (right-side inset). Antithetic, top-to-SE shear bands are locally observed shearing quartz veins or quartz-rich layers (left-side inset).

Figure 10 – Structural features of volcano-sedimentary rocks of southern Brusque Complex. (a) Sketch of uppermost layers from figure 9b. Asymmetric folds are developed over a carbonate-rich calc-silicatic layer and the schist, while boudinage affected the central epidote-rich calc-silicatic layer. (b) Detail from the central-upper portion of the figure 10a. The schist presents a banding given by biotite-rich (dark) and quartz-rich layers (light). Asymmetric folds given a top-to-the-NNW shear sense. The light bands are good

markers to identify the antithetic, discrete shear bands which affected the rocks later, with an opposite top-to-the-SSE shear sense (see inset). (c) Photograph from the NW extreme of the same uppermost sequence from figure 10a, showing the less competent, asymmetrically folded carbonate-rich calc-silicatic rock in the lower portion, and the boudinaged, epidote-rich calc-silicatic rock in the center, with the schist admixed with calc-silicatic thinner layers on the top. The very asymmetric shape of the folds in the lowermost strata changes wave-length and amplitude while it propagated upwards. The discontinuity between the layers acted as a rheological boundary, and the layer below the boudinaged one presents gently open folds bending in the boudin necks.. (d) Hand-specimen slab of a calc-silicatic, plagioclase-epidote-actinolite schist, presenting an asymmetricaly folded $S_{x,}$ which is interpreted as top-to-NNW shear sense. This fabric is reworked by a mylonitic foliation S_{x+1} defined by neocrystallization of biotite which anostomosed along the previous foliation and axial planes/long limbs, defining sigma-shaped pods of S_x with top-to-the-SSE shear sense. (e) Ramdomly growth porphyroblasts pseudomorphosed by white mica along certain schistosity levels (see figure 9b for location), indicative of static thermal metamorphism.

Fig. 11 – Contact between Brusque Complex amphibolites and Camboriú Complex mylonitic leucogranite in the Serra da Miséria. (a) Outcrop sketch (block-diagram) where both units present concordant mylonitic structures parallel to the contact. The mylonitic granite is locally intrusive in the amphibolites. Faults and fractures crosscut the contact at high-angle and a later-quartz vein is emplaced along these planes. (b) Stereonet presenting pole to foliation and lineation from both units, showing the concordance of attitudes. Lower hemisphere, equal area projection. BC – Brusque Complex; CC – Camboriú Complex; Sx – schistosity; Smil – mylonitic foliation; Lx – stretching lineation; Lamph – amphibole mineral lineation. (c) Horizontal view of the contact shown in the central upper portion of figure 11a. The left-side of the picture is the Camboriú Complex mylonitic leucogranite, which is lighter and coarse-grained if compared with Brusque Complex amphibolites, finer and darker. The concordant contact is observed and highlighted by erosional effects. A discordant vein of leucogranite with milky quartz crosscuts the amphibolite and merges with the mylonitic leucogranite in the upper portion of the picture. (d) Detail from a sheared quartz vein in

horizontal view, showing dextral apparent sense of shear. (e) Detail from a sheared quartz vein in vertical view, showing normal, or top-to-210° apparent sense of shear. (f) Photomicrograph (cross-polarized light) from a mylonitic leucogranite showing quartz and feldspar porphyroclasts surrounded by biotite + opaque and fine-grained quartz-rich recrystallized matrix (< 100 μm) showing apparent dextral asymmetry (top-to-250° - see inset; plan-polarized light). (g) Stereonet for mylonitic leucogranite quartz c-axis representing the population bigger than 100 μm. A girdle with clear apparent dextral asymmetry confirms the sense of shear identified at thin-section. (h) Stereonet for mylonitic leucogranite quartz c-axis representing the population smaller than 100 μm. The asymmetry is very similar to the first stereonet, but the distribution is more widespread, with a smaller maximum. Both stereonets are equal area, lower hemisphere projection, with reference frame parallel to the lineation (X) and perpendicular to the foliation (Z). See text for further details. (i) Slab from a fault-related rock handsample collected close to the detailed outcrop. It presents angular (cm-size) and rounded (mm-size) amphibolite fragments as block-in-matrix immerse in mylonitic quartz with different proportions of fine-grained, epidote-bearing, greenish material. (j) Fault-related rock photomicrograph presenting both the mylonitic leucogranite (left-side) and the amphibolite (righ-side), juxtaposed after cataclasis.

Fig. 12 – Camboriú Complex structures. (a) Stereonet for Itapema Granite contoured pole to foliation distribution (S_0 – magmatic foliation). Lower hemisphere, equal area projetction. (b) Itapema Granite general aspect, with magmatic banding given by different proportion of mafic minerals and gneissic xenoliths, enhanced by foliation-parallel leucocratic injections and pegmatites. (c) Migmatitic orthogneisses from Camboriú Complex presenting disharmonic folding. Notice that while some layers are boudinaged, others present high-mobility due to magmatic flow. (d) Stereonet for Camboriú Complex gneisses with contoured pole to foliation (Sb – main banding), stretching lineation (Lx), fold axis (B), axial plane (S_2) and conjugate shear bands attitudes. Lower hemisphere, equal area projection. (e) Detail from the center of figure 12c, where it is observed the mobility of leucosomes along fold limbs and sin-magmatic transposition shear bands along axial planes. (f) Folded granitoids among migmatitic gneisses from Camboriú Complex.

The foliation is enhanced by layer-parallel injections of fine-grained leucosomes which are folded together. Note that opposite limbs act as sin-magmatic shear bands of opposite shear sense, with the eastern limb acting as east-side down, while the western limb acted as west-side down, with vertical extrusion of the antiform hinge zone (subvertical exposure).

Figure 13 – Camboriú Complex metapelitic migmatite (CA-20Q) main petrographic characteristics. (a) Rock slab showing the relation and contrast between melanosome (mostly fine-grained, dark area, garnet-bearing, mafic-rich) and leucosome (coarser-grained, lens-like, light areas). (b) Photomicrograph of a garnet porphyroblast surrounded by both metamorphic and igneous minerals, as biotite and silimanite, and feldspar and quartz, respectively. Points of garnet chemical analysis are labeled. (c) Kyanite relict (dark gray at the center) partially replaced by silimanite (pink and blue to the right) and surrounded by quartz and biotite.

Fig. 14 – Pseudosection modeled for Camboriú Complex metapelitic migmatite (CA-20Q, system composition is presented in the heading). The curves for kyanite – sillimanite, cordierite-out and melt-in are shown. The isopleths for garnet pyrope (11 – 12%), grossular (2 – 3%) and spessartine (5 – 7%) are presented and constrain the range of 665 – 705°C and 4.35 – 5.3 kbar as equilibrium conditions.

Fig. 15 – PT diagram summarizing the estimatives for the three structural domains, with exhumation and heating paths correlated with previous published ages. Kyanite-sillimanite-andalusite and melt-in curves are from figure 14.

Fig. 16 – Tectonic evolution cartoon (not in scale). (a) Oblique collision early configuration (650 – 645 Ma). (b) Further transpression and infrastructure partial melting (645 – 635 Ma). (c) Strain partitioning and early post-collisional magmatism (636 – 615 Ma), with nucleation of Major Gercino Shear Zone. Strain partitioning leds exhumation of the Camboriú Complex and consequently extension of Brusque Complex

through the development of a dextral-normal detatchment, prior to Rio Pequeno Granite emplacement. (d) Strain partitioning and late post-collisional magmatism (615 – 600 Ma). (e) Finite deformation, after 600 Ma, which illustrates the actual configuration (based on figure 3). Zoom-in insets (yellow arrows) show examples of characteristic subhorizontal foliation preserved in the three structural domains. Horizontal and vertical scale are loosely mantained. (f) Deformation triangle (proposed by Jones et al., 2004) illustrating the kinematic partitioning of the area. Colours in this figure are the same as in figure 2 and 3.

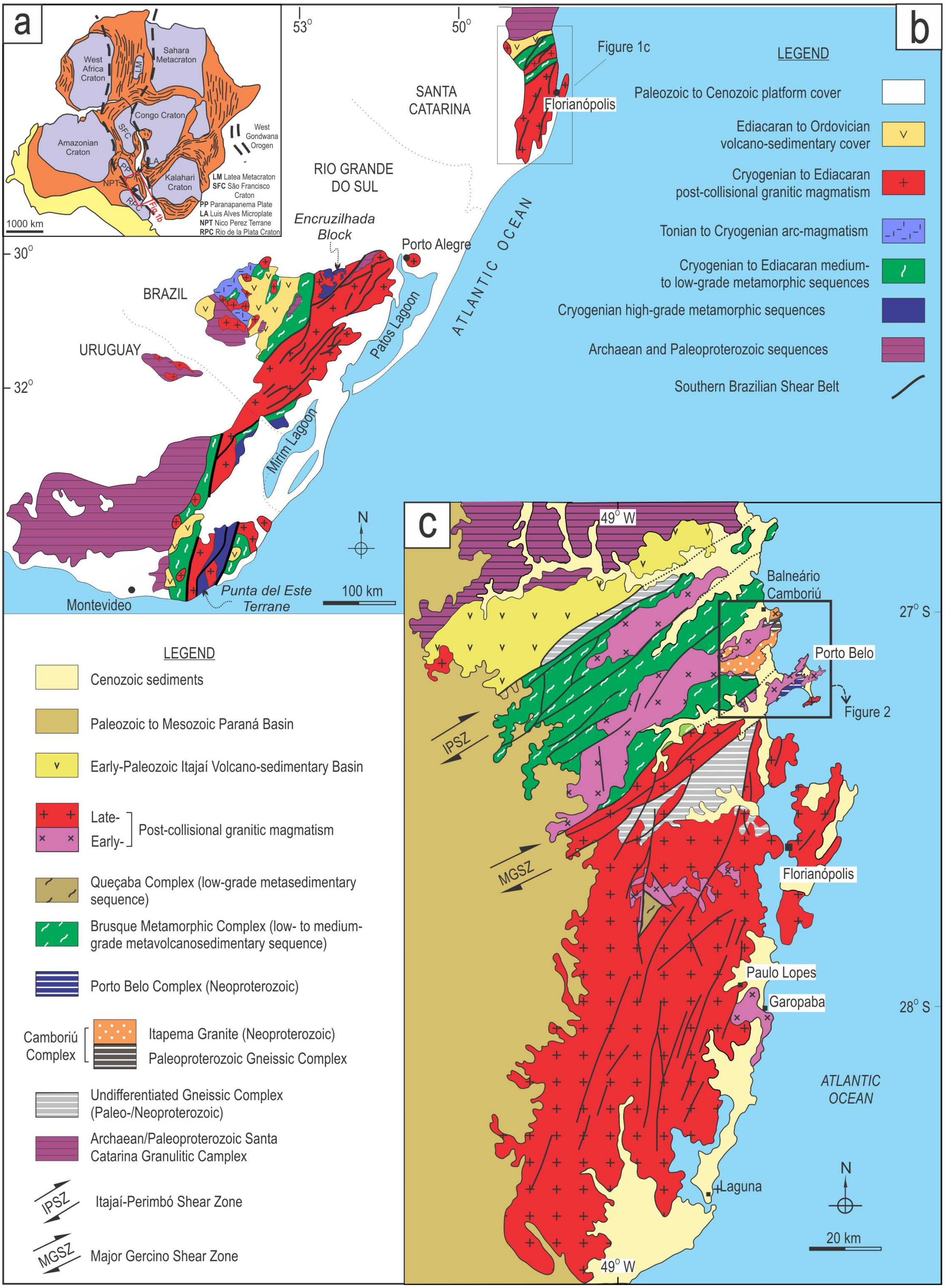
a
West Africa Craton
Sahara Metacraton
LM
Congo Craton
SFC
Amazonian Craton
West Gondwana Orogen
PP
LA
NPT
RPC
Kalahari Craton
LM Latea Metacraton
SFC São Francisco Craton
PP Paranapanema Plate
LA Luis Alves Microplate
NPT Nico Perez Terrane
RPC Rio de la Plata Craton
Fig 1b
1000 km
b
53°
50°
Figure 1c
Florianópolis
SANTA CATARINA
RIO GRANDE DO SUL
Encruzilhada Block
Porto Alegre
ATLANTIC OCEAN
Patos Lagoon
Mirim Lagoon
BRAZIL
URUGUAY
30°
32°
Montevideo
Punta del Este Terrane
100 km
N
LEGEND
Paleozoic to Cenozoic platform cover
Ediacaran to Ordovician volcano-sedimentary cover
Cryogenian to Ediacaran post-collisional granitic magmatism
Tonian to Cryogenian arc-magmatism
Cryogenian to Ediacaran medium- to low-grade metamorphic sequences
Cryogenian high-grade metamorphic sequences
Archaean and Paleoproterozoic sequences
Southern Brazilian Shear Belt
c
49° W
Balneário Camboriú
27° S
Porto Belo
Figure 2
IPSZ
MGSZ
Florianópolis
Paulo Lopes
Garopaba
28° S
ATLANTIC OCEAN
Laguna
N
20 km
49° W
LEGEND
Cenozoic sediments
Paleozoic to Mesozoic Paraná Basin
Early-Paleozoic Itajaí Volcano-sedimentary Basin
Late-
Early-
Post-collisional granitic magmatism
Queçaba Complex (low-grade metasedimentary sequence)
Brusque Metamorphic Complex (low- to medium-grade metavolcanosedimentary sequence)
Porto Belo Complex (Neoproterozoic)
Camboriú Complex
Itapema Granite (Neoproterozoic)
Paleoproterozoic Gneissic Complex
Undifferentiated Gneissic Complex (Paleo-/Neoproterozoic)
Archaean/Paleoproterozoic Santa Catarina Granulitic Camplex
IPSZ Itajaí-Perimbó Shear Zone
MGSZ Major Gercino Shear Zone

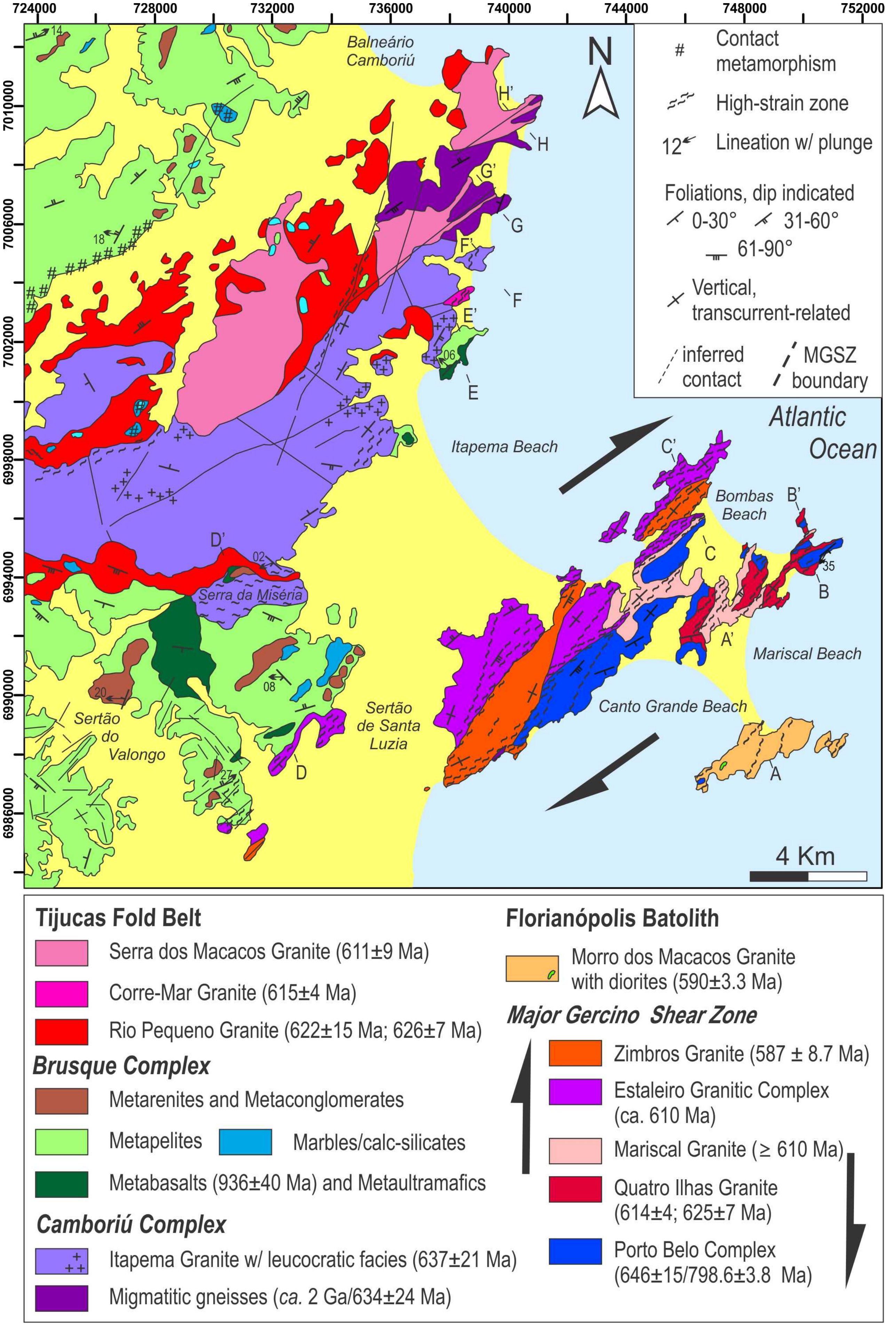
724000
728000
732000
736000
740000
744000
748000
752000
7010000
7006000
7002000
6998000
6994000
6990000
6986000
Balneário Camboriú
N
Contact metamorphism
High-strain zone
12 Lineation w/ plunge
Foliations, dip indicated
0-30°
31-60°
61-90°
Vertical, transcurrent-related
inferred contact
MGSZ boundary
Atlantic Ocean
Itapema Beach
Bombas Beach
Mariscal Beach
Canto Grande Beach
Serra da Miséria
Sertão do Valongo
Sertão de Santa Luzia
A
A'
B
B'
C
C'
D
D'
E
E'
F
F'
G
G'
H
H'
14
18
02
06
08
20
27
35
4 Km
Tijucas Fold Belt
Serra dos Macacos Granite (611±9 Ma)
Corre-Mar Granite (615±4 Ma)
Rio Pequeno Granite (622±15 Ma; 626±7 Ma)
Brusque Complex
Metarenites and Metaconglomerates
Metapelites
Marbles/calc-silicates
Metabasalts (936±40 Ma) and Metaultramafics
Camboriú Complex
Itapema Granite w/ leucocratic facies (637±21 Ma)
Migmatitic gneisses (ca. 2 Ga/634±24 Ma)
Florianópolis Batolith
Morro dos Macacos Granite with diorites (590±3.3 Ma)
Major Gercino Shear Zone
Zimbros Granite (587 ± 8.7 Ma)
Estaleiro Granitic Complex (ca. 610 Ma)
Mariscal Granite (≥ 610 Ma)
Quatro Ilhas Granite (614±4; 625±7 Ma)
Porto Belo Complex (646±15/798.6±3.8 Ma)

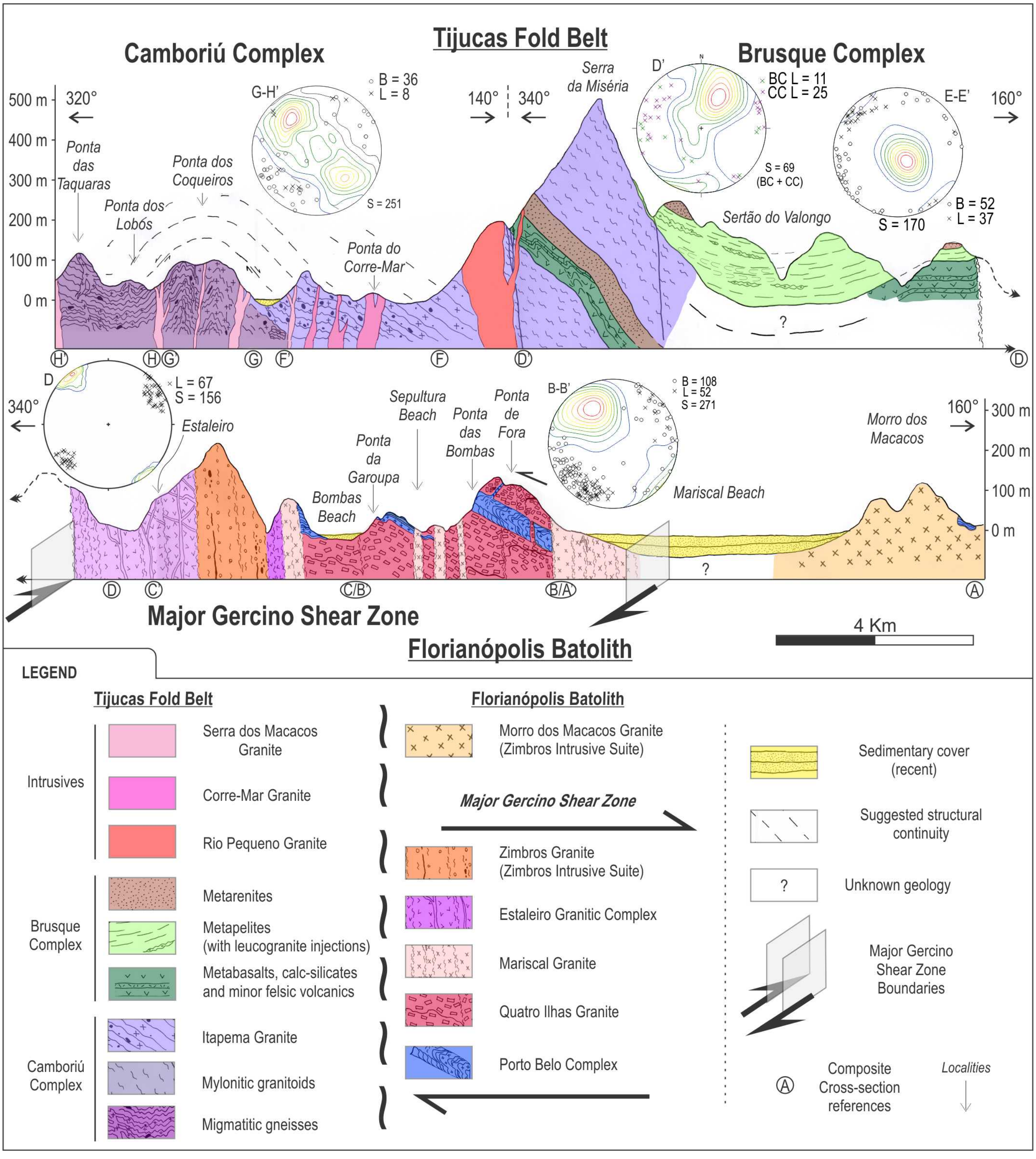

Tijucas Fold Belt
Camboriú Complex
Brusque Complex
500 m
400 m
300 m
200 m
100 m
0 m
320°
140°
340°
160°
G-H'
B = 36
L = 8
S = 251
Ponta das Taquaras
Ponta dos Lobos
Ponta dos Coqueiros
Ponta do Corre-Mar
Serra da Miséria
D'
BC L = 11
CC L = 25
S = 69
(BC + CC)
E-E'
B = 52
L = 37
S = 170
Sertão do Valongo
?
H
H' G'
G
F'
F
D'
D
D
L = 67
S = 156
340°
Estaleiro
Sepultura Beach
Ponta da Garoupa
Bombas Beach
Ponta das Bombas
Ponta de Fora
B-B'
B = 108
L = 52
S = 271
Mariscal Beach
Morro dos Macacos
160°
300 m
200 m
100 m
0 m
?
D
C
C/B
B/A
A
Major Gercino Shear Zone
Florianópolis Batolith
4 Km
LEGEND
Tijucas Fold Belt
Intrusives
Serra dos Macacos Granite
Corre-Mar Granite
Rio Pequeno Granite
Brusque Complex
Metarenites
Metapelites (with leucogranite injections)
Metabasalts, calc-silicates and minor felsic volcanics
Camboriú Complex
Itapema Granite
Mylonitic granitoids
Migmatitic gneisses
Florianópolis Batolith
Morro dos Macacos Granite (Zimbros Intrusive Suite)
Major Gercino Shear Zone
Zimbros Granite (Zimbros Intrusive Suite)
Estaleiro Granitic Complex
Mariscal Granite
Quatro Ilhas Granite
Porto Belo Complex
Sedimentary cover (recent)
Suggested structural continuity
?
Unknown geology
Major Gercino Shear Zone Boundaries
A
Composite Cross-section references
Localities

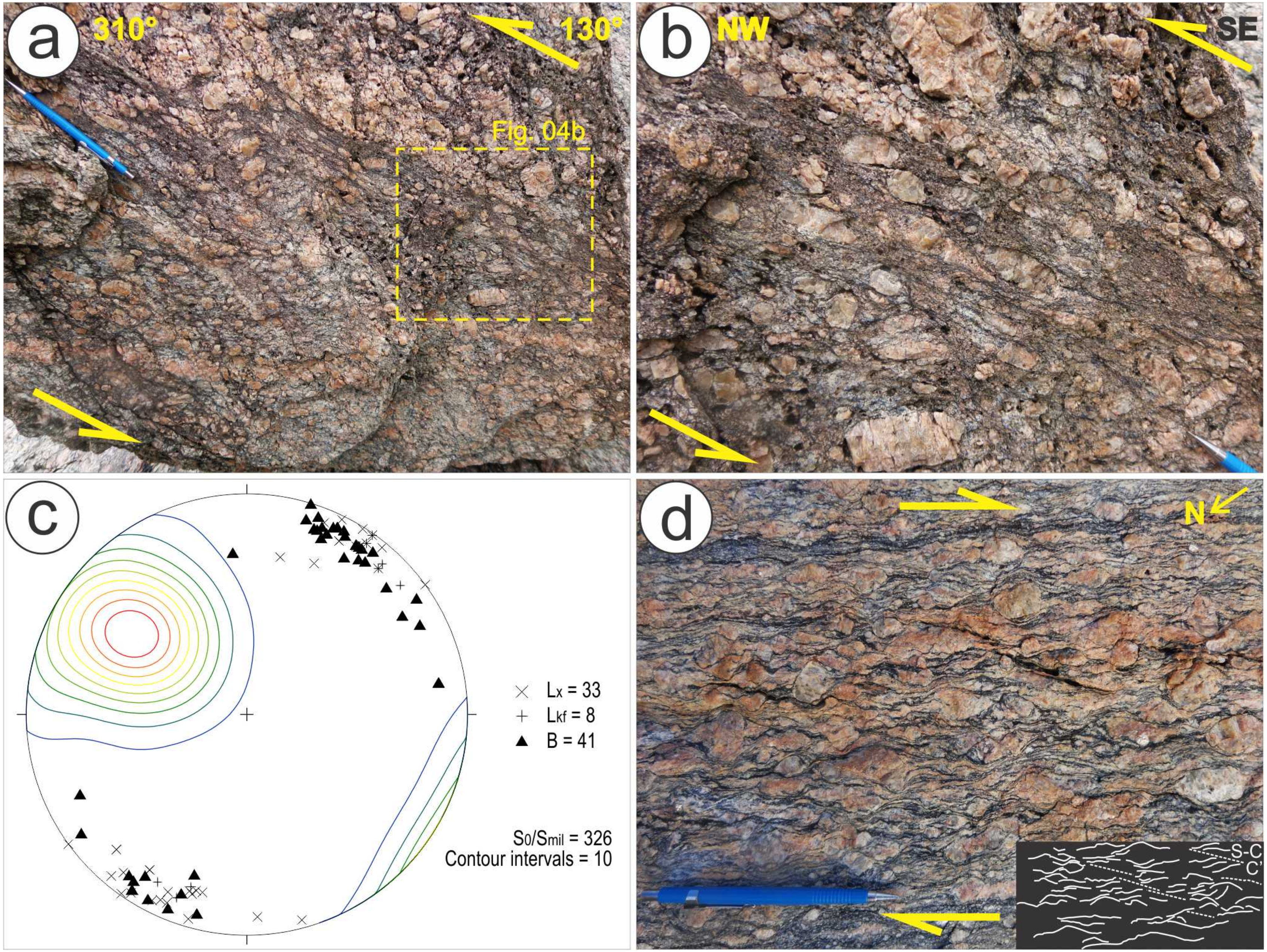

a
310°
130°
Fig. 04b
b
NW
SE
c
Lx = 33
Lkf = 8
B = 41
S0/Smil = 326
Contour intervals = 10
d
N
S-C
C'

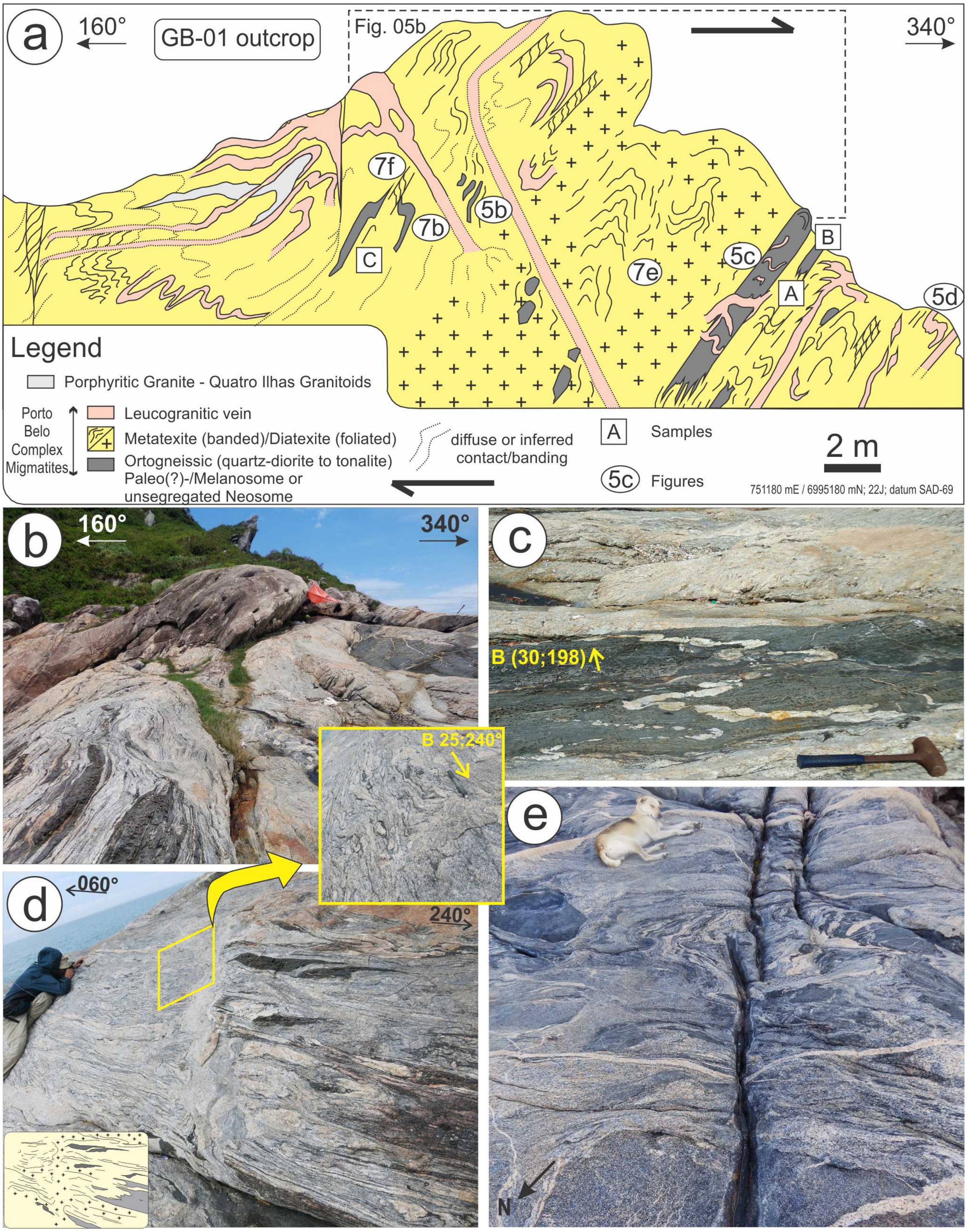
a
160°
GB-01 outcrop
Fig. 05b
340°
7f
5b
7b
C
B
5c
7e
A
5d
Legend
Porphyritic Granite - Quatro Ilhas Granitoids
Porto Belo Complex Migmatites
Leucogranitic vein
Metatexite (banded)/Diatexite (foliated)
Ortogneissic (quartz-diorite to tonalite) Paleo(?)-/Melanosome or unsegregated Neosome
diffuse or inferred contact/banding
A Samples
5c Figures
2 m
751180 mE / 6995180 mN; 22J; datum SAD-69
b
160°
340°
B 25;240°
c
B (30;198)
d
060°
240°
e
N

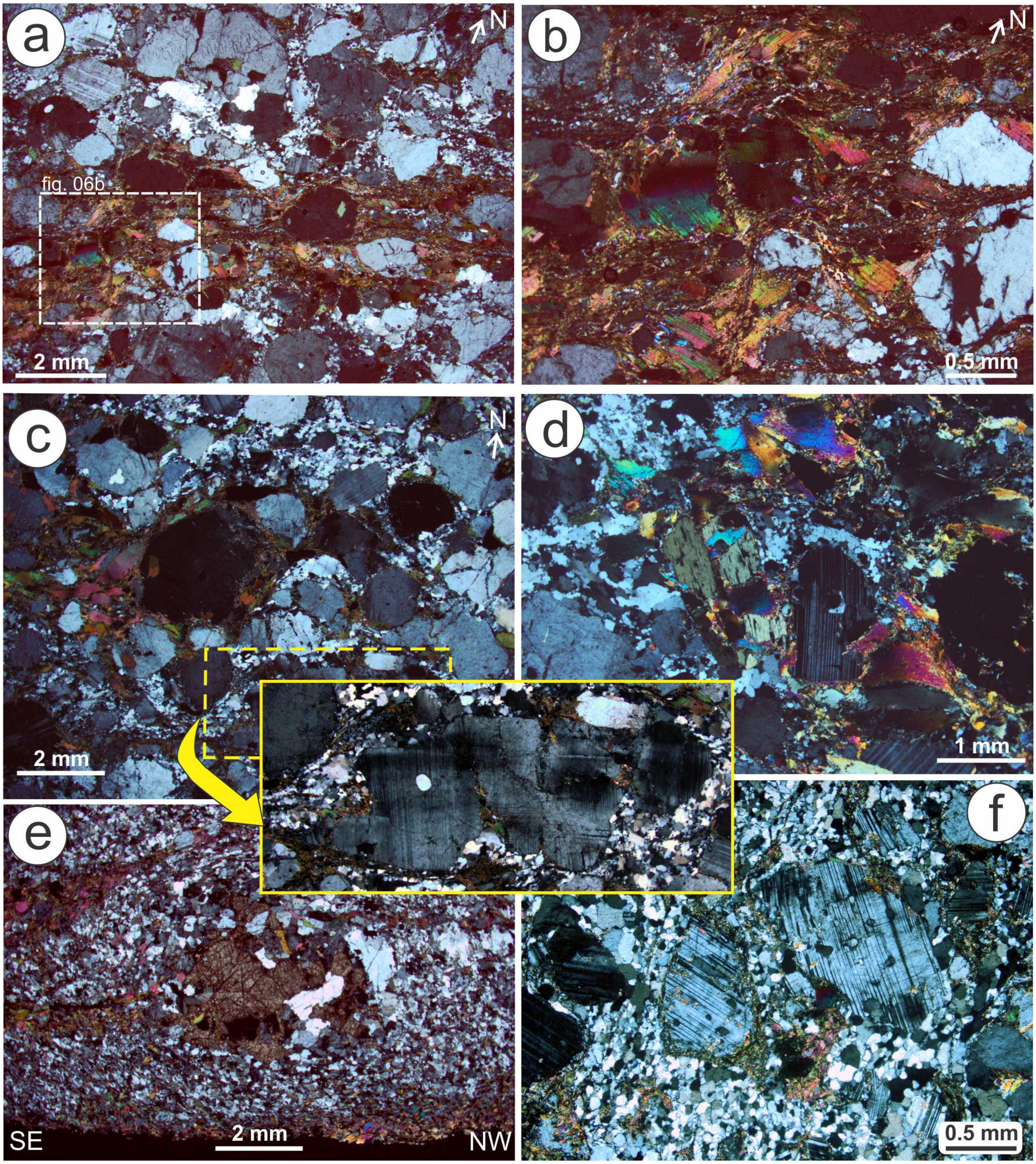
a
N
fig. 06b
2 mm
b
N
0.5 mm
c
N
2 mm
d
1 mm
e
SE
2 mm
NW
f
0.5 mm

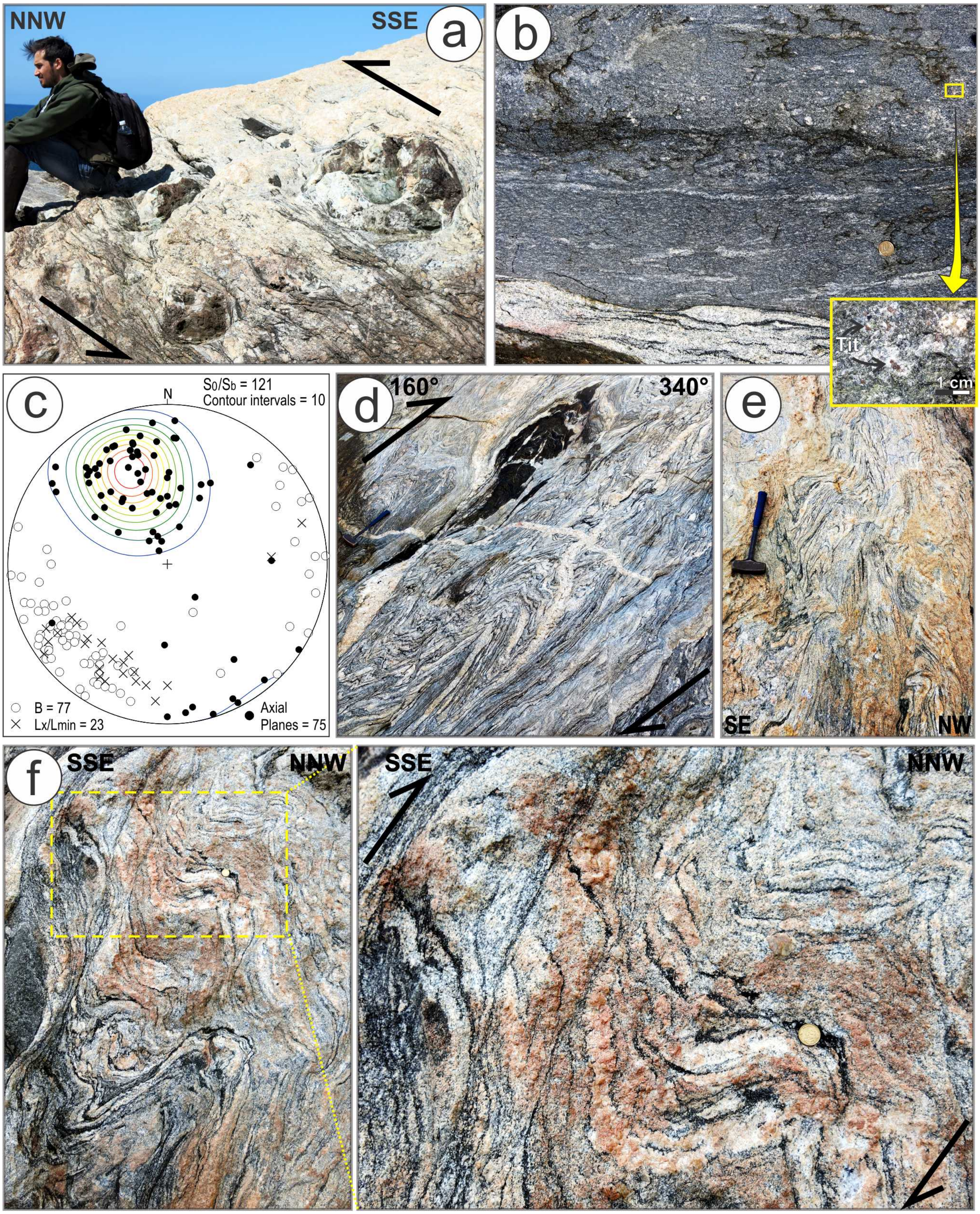
a
NNW
SSE
b
Tit
1 cm
c
S0/Sb = 121
Contour intervals = 10
N
B = 77
Lx/Lmin = 23
Axial Planes = 75
d
160°
340°
e
SE
NW
f
SSE
NNW
SSE
NNW

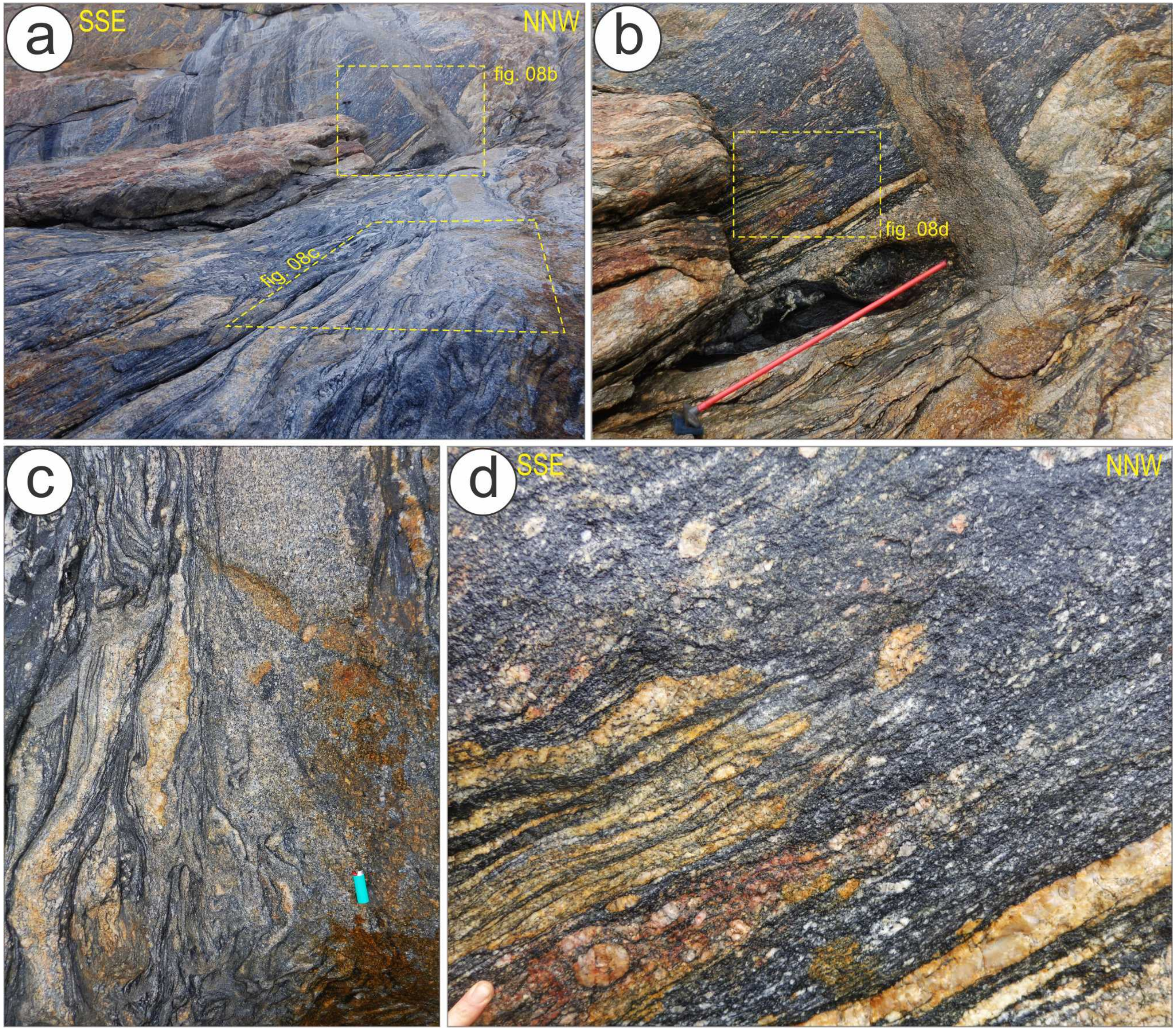
a
SSE
NNW
fig. 08b
fig. 08c
b
fig. 08d
c
d
SSE
NNW

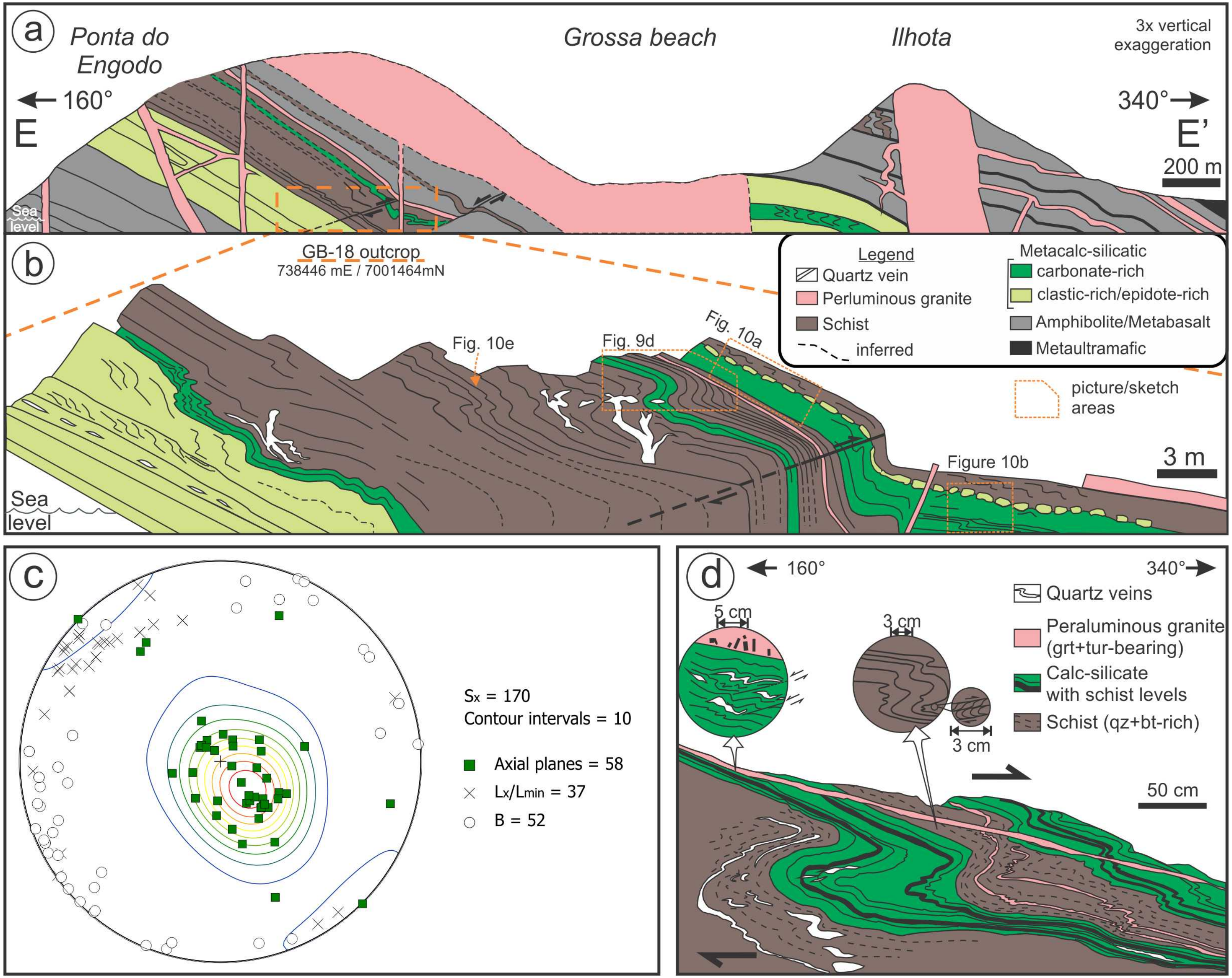

a
Ponta do Engodo
Grossa beach
Ilhota
3x vertical exaggeration
← 160°
E
340° →
E'
200 m
Sea level
b
GB-18 outcrop
738446 mE / 7001464mN
Legend
Quartz vein
Perluminous granite
Schist
inferred
Metacalc-silicatic
carbonate-rich
clastic-rich/epidote-rich
Amphibolite/Metabasalt
Metaultramafic
picture/sketch areas
Fig. 10e
Fig. 9d
Fig. 10a
Figure 10b
3 m
Sea level
c
Sx = 170
Contour intervals = 10
Axial planes = 58
Lx/Lmin = 37
B = 52
d
160°
340°
Quartz veins
Peraluminous granite (grt+tur-bearing)
Calc-silicate with schist levels
Schist (qz+bt-rich)
5 cm
3 cm
3 cm
50 cm

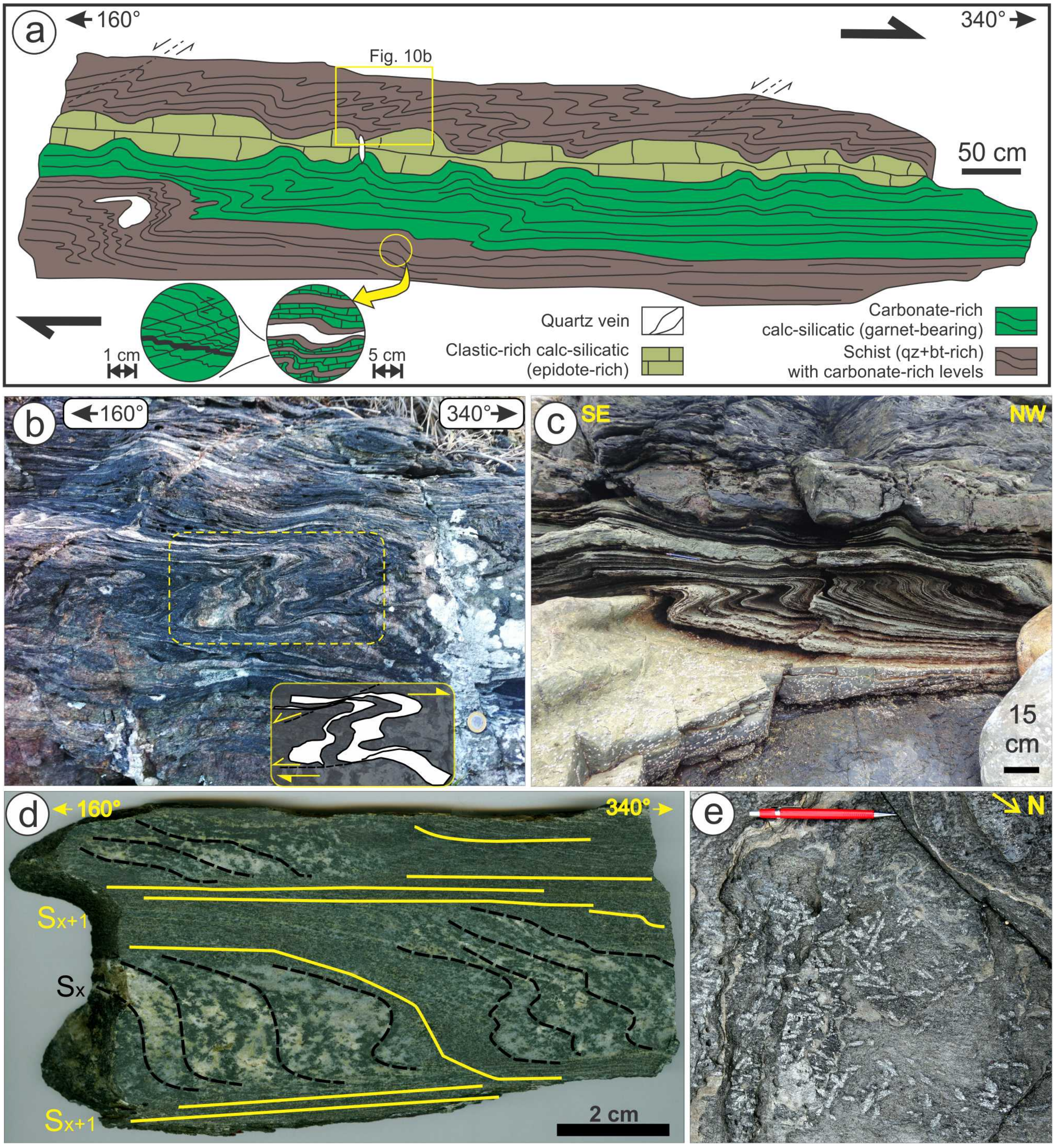

a
160°
340°
Fig. 10b
50 cm
1 cm
5 cm
Quartz vein
Clastic-rich calc-silicatic
(epidote-rich)
Carbonate-rich
calc-silicatic (garnet-bearing)
Schist (qz+bt-rich)
with carbonate-rich levels
b
160°
340°
c
SE
NW
15
cm
d
160°
340°
S_{x+1}
S_x
S_{x+1}
2 cm
e
N

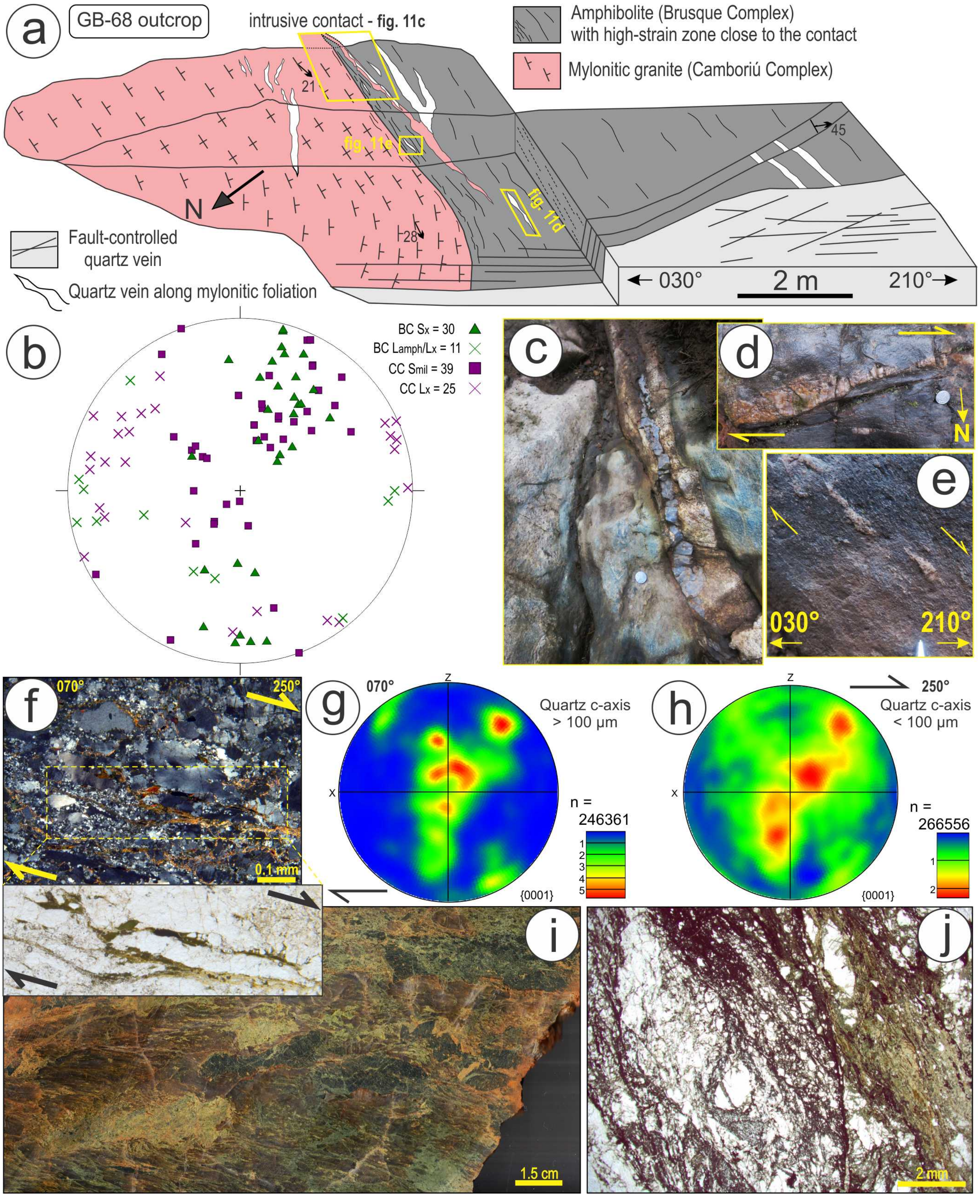
a
GB-68 outcrop
intrusive contact - fig. 11c
Amphibolite (Brusque Complex)
with high-strain zone close to the contact
Mylonitic granite (Camboriú Complex)
21
fig. 11e
fig. 11d
45
N
28
Fault-controlled
quartz vein
Quartz vein along mylonitic foliation
030°
2 m
210°
b
BC Sx = 30
BC Lamph/Lx = 11
CC Smil = 39
CC Lx = 25
c
d
N
e
030°
210°
f
070°
250°
0.1 mm
g
070°
Quartz c-axis
> 100 µm
n =
246361
{0001}
h
250°
Quartz c-axis
< 100 µm
n =
266556
{0001}
i
1.5 cm
j
2 mm

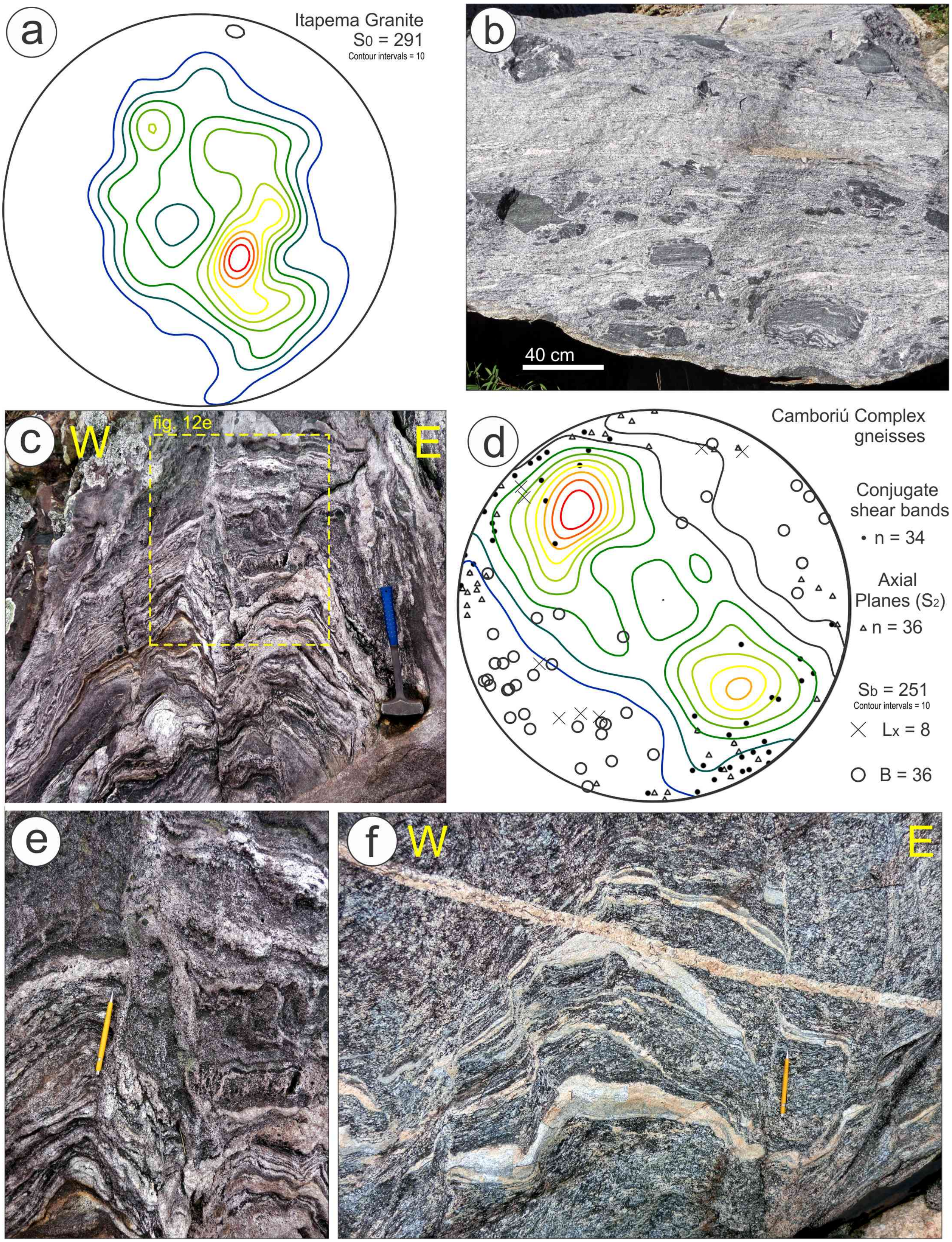

a
Itapema Granite
S_0 = 291
Contour intervals = 10
b
40 cm
c
W
fig. 12e
E
d
Camboriú Complex
gneisses
Conjugate
shear bands
n = 34
Axial
Planes (S_2)
n = 36
S_b = 251
Contour intervals = 10
L_x = 8
B = 36
e
f
W
E

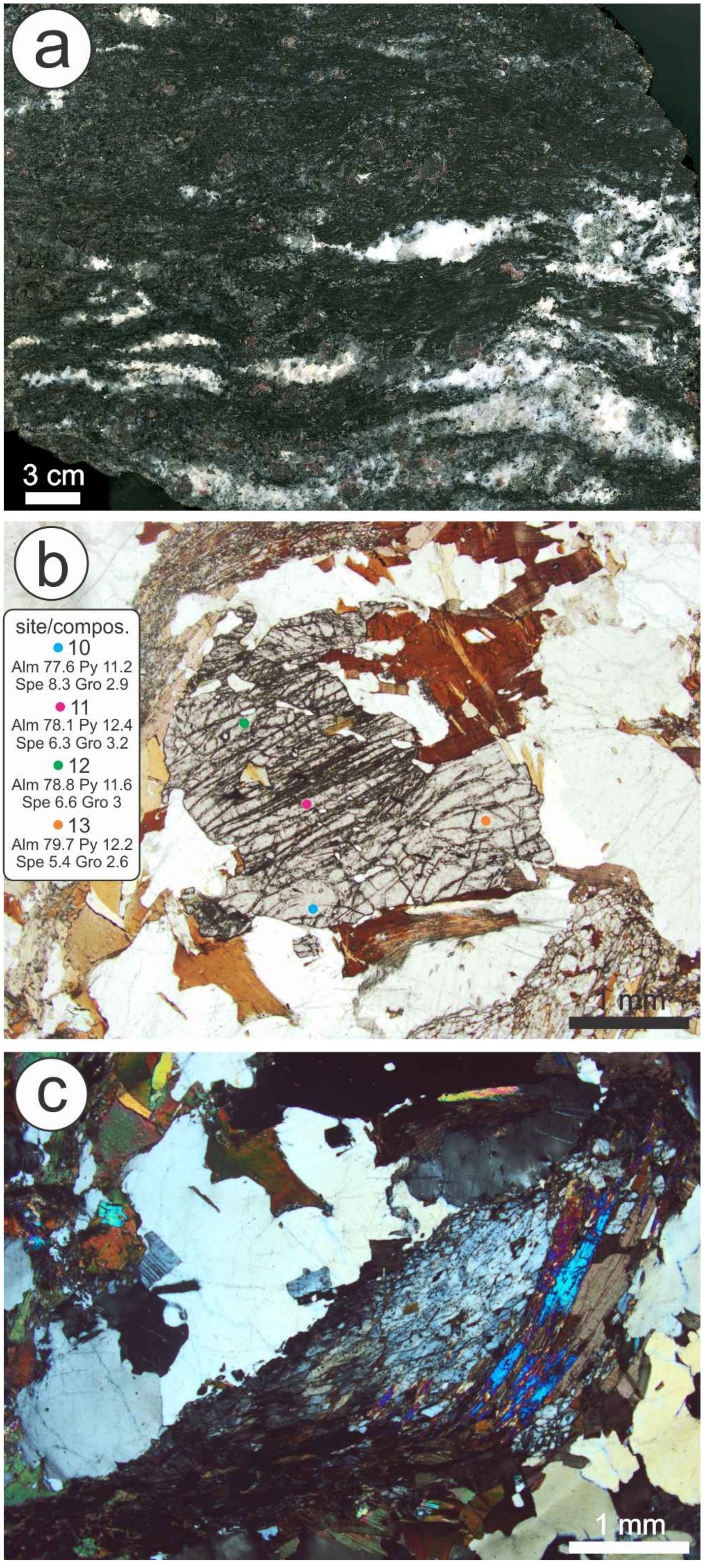
a
3 cm
b
site/compos.
10
Alm 77.6 Py 11.2
Spe 8.3 Gro 2.9
11
Alm 78.1 Py 12.4
Spe 6.3 Gro 3.2
12
Alm 78.8 Py 11.6
Spe 6.6 Gro 3
13
Alm 79.7 Py 12.2
Spe 5.4 Gro 2.6
1 mm
c
1 mm

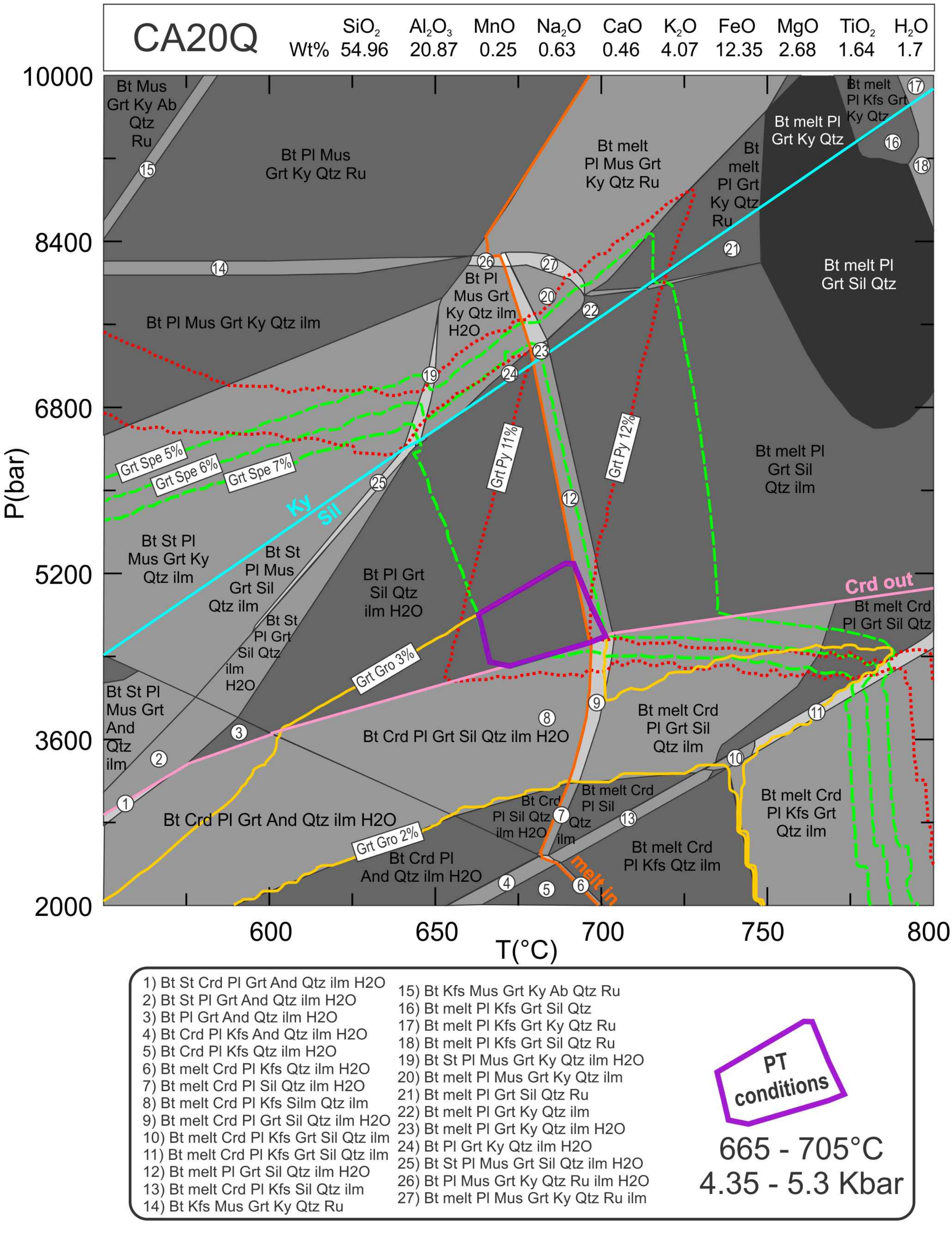

CA20Q
Wt% SiO2 54.96 Al2O3 20.87 MnO 0.25 Na2O 0.63 CaO 0.46 K2O 4.07 FeO 12.35 MgO 2.68 TiO2 1.64 H2O 1.7
P(bar)
T(°C)
10000
8400
6800
5200
3600
2000
600
650
700
750
800
Ky
Sil
Crd out
melt in
Grt Spe 5%
Grt Spe 6%
Grt Spe 7%
Grt Py 11%
Grt Py 12%
Grt Gro 3%
Grt Gro 2%
Bt Mus Grt Ky Ab Qtz Ru
Bt Pl Mus Grt Ky Qtz Ru
Bt melt Pl Mus Grt Ky Qtz Ru
Bt melt Pl Grt Ky Qtz Ru
Bt melt Pl Grt Ky Qtz
Bt melt Pl Kfs Grt Ky Qtz
Bt melt Pl Grt Sil Qtz
Bt Pl Mus Grt Ky Qtz ilm
Bt Pl Mus Grt Ky Qtz ilm H2O
Bt St Pl Mus Grt Ky Qtz ilm
Bt St Pl Mus Grt Sil Qtz ilm
Bt St Pl Grt Sil Qtz ilm H2O
Bt Pl Grt Sil Qtz ilm H2O
Bt melt Pl Grt Sil Qtz ilm
Bt melt Crd Pl Grt Sil Qtz
Bt St Pl Mus Grt And Qtz ilm
Bt Crd Pl Grt Sil Qtz ilm H2O
Bt melt Crd Pl Grt Sil Qtz ilm
Bt Crd Pl Grt And Qtz ilm H2O
Bt Crd Pl Sil Qtz ilm H2O
Bt melt Crd Pl Sil Qtz ilm
Bt Crd Pl And Qtz ilm H2O
Bt melt Crd Pl Kfs Qtz ilm
Bt melt Crd Pl Kfs Grt Qtz ilm
1) Bt St Crd Pl Grt And Qtz ilm H2O
2) Bt St Pl Grt And Qtz ilm H2O
3) Bt Pl Grt And Qtz ilm H2O
4) Bt Crd Pl Kfs And Qtz ilm H2O
5) Bt Crd Pl Kfs Qtz ilm H2O
6) Bt melt Crd Pl Kfs Qtz ilm H2O
7) Bt melt Crd Pl Sil Qtz ilm H2O
8) Bt melt Crd Pl Kfs Silm Qtz ilm
9) Bt melt Crd Pl Grt Sil Qtz ilm H2O
10) Bt melt Crd Pl Kfs Grt Sil Qtz ilm
11) Bt melt Crd Pl Kfs Grt Sil Qtz ilm
12) Bt melt Pl Grt Sil Qtz ilm H2O
13) Bt melt Crd Pl Kfs Sil Qtz ilm
14) Bt Kfs Mus Grt Ky Qtz Ru
15) Bt Kfs Mus Grt Ky Ab Qtz Ru
16) Bt melt Pl Kfs Grt Sil Qtz
17) Bt melt Pl Kfs Grt Ky Qtz Ru
18) Bt melt Pl Kfs Grt Sil Qtz Ru
19) Bt St Pl Mus Grt Ky Qtz ilm H2O
20) Bt melt Pl Mus Grt Ky Qtz ilm
21) Bt melt Pl Grt Sil Qtz Ru
22) Bt melt Pl Grt Ky Qtz ilm
23) Bt melt Pl Grt Ky Qtz ilm H2O
24) Bt Pl Grt Ky Qtz ilm H2O
25) Bt St Pl Mus Grt Sil Qtz ilm H2O
26) Bt Pl Mus Grt Ky Qtz Ru ilm H2O
27) Bt melt Pl Mus Grt Ky Qtz Ru ilm
PT conditions
665 - 705°C
4.35 - 5.3 Kbar

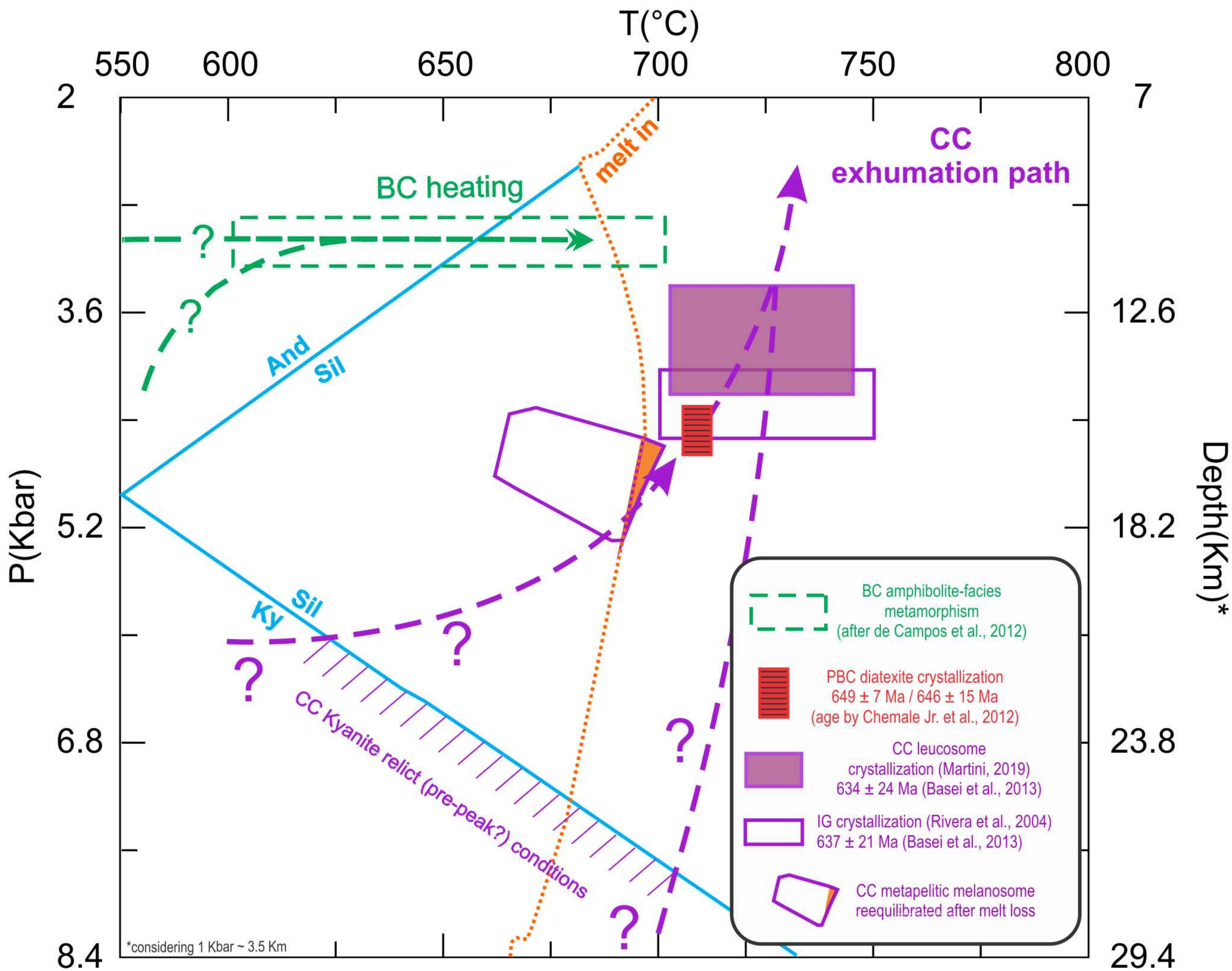
T(°C)
550
600
650
700
750
800
2
3.6
5.2
6.8
8.4
7
12.6
18.2
23.8
29.4
P(Kbar)
Depth(Km)*
melt in
BC heating
CC
exhumation path
And
Sil
Sil
Ky
CC Kyanite relict (pre-peak?) conditions
*considering 1 Kbar ~ 3.5 Km
BC amphibolite-facies metamorphism (after de Campos et al., 2012)
PBC diatexite crystallization 649 ± 7 Ma / 646 ± 15 Ma (age by Chemale Jr. et al., 2012)
CC leucosome crystallization (Martini, 2019) 634 ± 24 Ma (Basei et al., 2013)
IG crystallization (Rivera et al., 2004) 637 ± 21 Ma (Basei et al., 2013)
CC metapelitic melanosome reequilibrated after melt loss

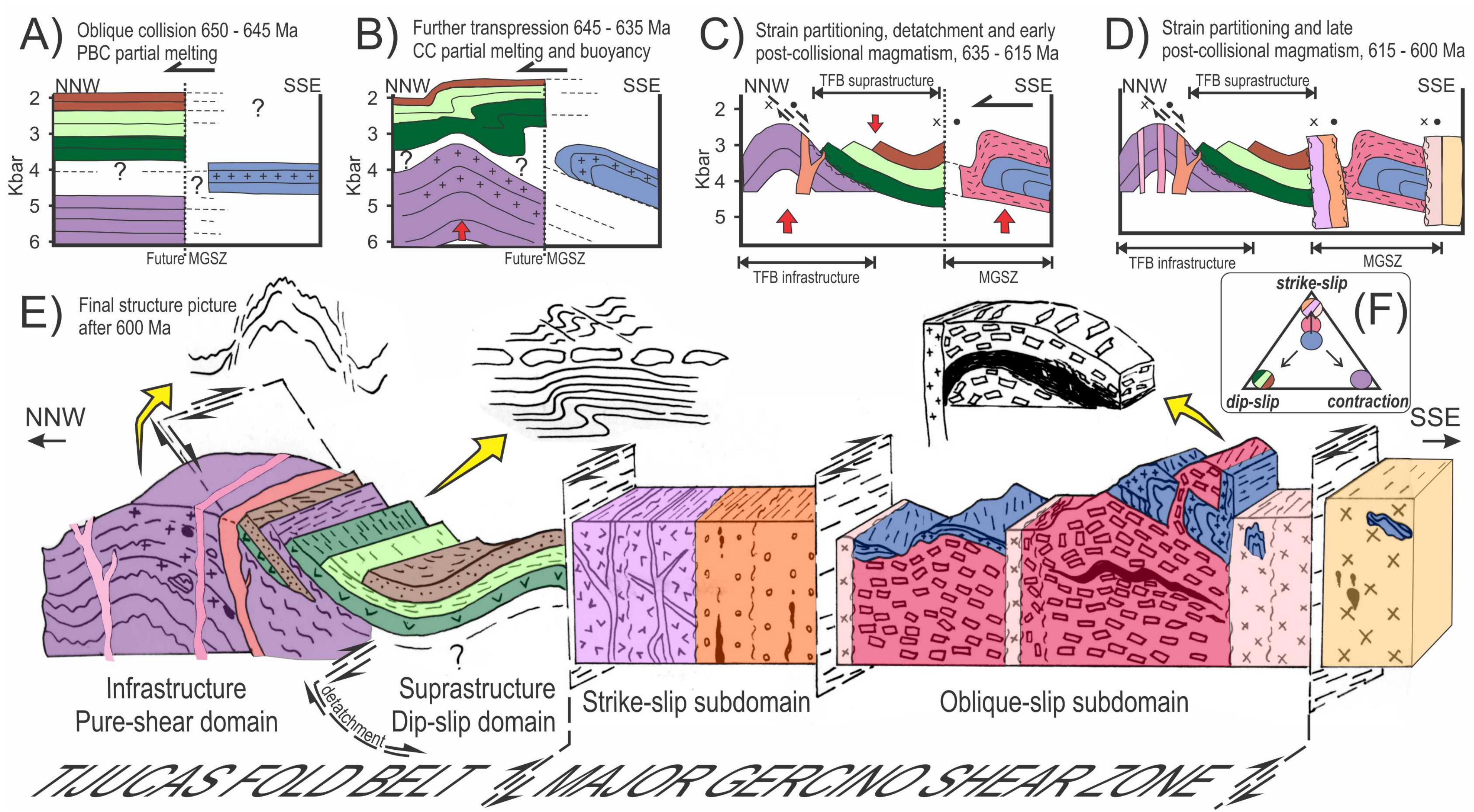
A) Oblique collision 650 - 645 Ma
PBC partial melting
NNW
SSE
Kbar
2
3
4
5
6
?
?
?
Future MGSZ
B) Further transpression 645 - 635 Ma
CC partial melting and buoyancy
NNW
SSE
Kbar
?
?
Future MGSZ
C) Strain partitioning, detatchment and early
post-collisional magmatism, 635 - 615 Ma
NNW
TFB suprastructure
SSE
Kbar
TFB infrastructure
MGSZ
D) Strain partitioning and late
post-collisional magmatism, 615 - 600 Ma
NNW
TFB suprastructure
SSE
TFB infrastructure
MGSZ
E) Final structure picture
after 600 Ma
NNW
SSE
strike-slip
(F)
dip-slip
contraction
?
Infrastructure
Pure-shear domain
detatchment
Suprastructure
Dip-slip domain
Strike-slip subdomain
Oblique-slip subdomain
TIJUCAS FOLD BELT
MAJOR GERCINO SHEAR ZONE

Declaration of interests

 The authors declare that they have no known competing financial interests or personal relationships that could have appeared to influence the work reported in this paper.

☐The authors declare the following financial interests/personal relationships which may be considered as potential competing interests:

Giuseppe De Toni: Conceptualization, Methodology, Writing - Original Draft

Maria de Fátima Bitencourt: Supervision, Writing - Original Draft, Funding acquisition, Project administration

Jiri Konopasek: Validation, Supervision, Writing - Review & Editing, Funding acquisition, Project administration

Amós Martini: Investigation

Pedro Andrade: Investigation

Luana Florisbal: Investigation, Resources

Roberto de Campos: Investigation